PET Perfusion Imaging and Nuclear Cardiology

K. Lance Gould

Division of Cardiology and the Positron Diagnostic and Research Center, The University of Texas Health Science Center at Houston, Houston, Texas.

J Nucl Med 1991; 32:579–606

Nuclear cardiology has evolved through several important stages. Initial methods utilized single or paired coincident detectors to record a first pass radioangiogram or decay curves reflecting global myocardial perfusion. The next stage evolved to planar imaging of myocardial perfusion during treadmill exercise with thallium-201, which became a widespread clinical tool as did gated blood-pool imaging for left ventricular function. Planar imaging evolved to single-photon emission computed tomography (SPECT). Dipyridamole has been documented as a substitute for exercise stress. Positron emission tomography (PET) of the heart branched off from earlier developing brain PET at several centers utilizing cyclotron-produced radionuclides developed originally for brain studies. However, the complexity, expense, and low patient volume of cyclotron-based PET has kept it primarily a research tool at large university centers. Nuclear cardiology is now well into its most advanced stage of development using an economical, generator-produced radionuclide, rubidium-82, with fast PET scanners designed to acquire adequate counts for diagnostic images in the brief acquisition times available for a short half-life tracer (75 sec).

This final step in advanced technology brings nuclear cardiology into a phase of widespread, readily available, clinical PET, providing hard, independent data comparable in reliability and diagnostic value to the coronary arteriogram (*1*). This review outlines current clinical cardiac PET as the mainstream evolution of nuclear cardiology into routine, high-volume, generator-based, PET applications for accurate diagnosis of coronary artery disease or assessment of its severity and extent of viable myocardium as a basis for medical or mechanical intervention.

SCOPE OF THE CLINICAL PROBLEM

Coronary heart disease causes 1.5 million myocardial infarctions and 520,000 deaths per year (one-third to one-half of deaths between the ages of 35 and 64) in the United States (*1,2*). Up to 13% of middle-aged men in the general population have coronary atherosclerosis, most of it clinically silent (*3,4*). Silent myocardial ischemia is increasingly recognized in symptomatic and asymptomatic individuals (*5–14*). It has an unfavorable prognosis when occurring during exercise testing (*7*) in patients with recent unstable angina (*8*) or in asymptomatic patients with perfusion defects after dipyridamole (*11–14*). Up to 48% of asymptomatic subjects with silent ischemia have a cardiac event (angina pectoris, myocardial infarction, or sudden death) within 4–6 yr (*7,9*). Forty to 60% of patients with sudden death or myocardial infarction present no previous symptoms (*15–18*). Therefore, silent coronary atherosclerosis remains a particular problem in cardiovascular medicine because there are no warning symptoms until a major cardiac event occurs.

The major questions for cardiovascular medicine are how to identify silent coronary artery disease (CAD) in specific individuals, how to define its severity in either the symptomatic or asymptomatic patient, how to decide objectively among dietary, medical, and mechanical interventions, how to assess the results invasively and noninvasively, and how to reduce unnecessary invasive procedures by accurately selecting appropriate patients. At the other end of the clinical spectrum, in patients with myocardial infarction and myocardial salvage by thrombolysis, percutaneous transluminal coronary angioplasty (PTCA) or bypass surgery requires reliable measures of myocardial viability and involvement of other coronary arteries to determine definitive mechanical interventions having significant risks.

RISK FACTORS FOR CAD

With widespread cholesterol testing, many individuals are identified as having risk factors for coronary atherosclerosis. However, risk factors do not accurately correlate with or identify individuals with symptomatic or asymptomatic CAD. For example, two-thirds of men aged 40–55 with high cholesterol and blood pressure remain well over the subsequent 25 yr (*19*), whereas one-third develop coronary heart disease. In asymptomatic males of this age group with risk factors, coronary arteriography shows disease in 15%–35% (*1–4,20–22*) that is anatomically severe in 7%–35% (*1,2,21*). Of asymptomatic middle-aged men who have a positive ECG exercise test, only 30%–43% have significant CAD by arteriography (*2*) and 5%–46%

Received Sept. 15, 1990; revision accepted Jan. 17, 1991.

For reprints contact: K. Lance Gould, MD, Box 20708, Room 4.258, Division of Cardiology, University of Texas Medical School at Houston, Houston, Texas 77225.

(mean 25%) develop clinical disease over the next 13–25 years (*2,19*). Therefore, approximately two-thirds of men are resistant to clinical CAD despite having risk factors, whereas one-third have or develop it, often with only modestly elevated or normal cholesterol levels. Consequently, high-risk patients commonly undergo coronary arteriography at some risk and considerable health care costs in order to confirm normal coronary arteries, particularly after false-positive exercise testing. A substantial number of patients with risk factors are treated with expensive lipid-lowering drugs at some risk, despite a large proportion of such patients who do not have or will not develop coronary atherosclerosis.

PET

Cardiac PET accurately identifies and assesses severity of coronary artery stenosis and myocardial viability as a basis for choosing and following effects of interventions, including risk factor management, pharmacologic agents, PTCA, thrombolysis, and bypass surgery. Accurate noninvasive identification and quantitation are particularly important in silent CAD as the only criteria for intervention to prevent sudden death or acute myocardial infarction.

Cardiac PET is not only a reliable guide to managing CAD in traditional cardiology practice based on symptoms; it also provides the basis for vigorous medical or mechanical management of asymptomatic coronary atherosclerosis. Such accurate noninvasive evaluation by PET is intended to identify individuals who need cardiac catheterization and to avoid unnecessary procedures in patients with either mild or no coronary artery disease suitable for reversal therapy, as subsequently reviewed. Cardiac PET interfaces positively with invasive cardiology by making its application more efficient and selective.

Physiologic basis, technology, major clinical applications, and extensive case studies have been recently described in the first text of cardiac PET (*1*).

BASIC PET PRINCIPLES

A positron is a positively-charged electron emitted by unstable atoms in the process of radioactive decay, such as generator-produced rubidium-82 or cyclotron-produced carbon-11, oxygen-15, nitrogen-13, and fluorine-18. This positron travels several mm through tissue and annihilates with a negative electron, giving off two 511-keV photons in opposite directions. The annihilation photon pair can be detected with a pair of radiation detectors connected through a coincidence-counting circuit, so that one decay is recorded if both detectors are activated simultaneously by the photon pair.

Radioactive decays occurring outside the sample volume between the detectors are excluded from the count data since an unpaired photon striking only one of the detectors is not counted. Collimation, or exclusion of stray radiation, is therefore accomplished electronically with coincidence counting rather than solely with lead collimators, as in single-photon imaging. Coincidence counting has several attributes that make PET uniquely quantitative and accurate for clinical imaging, including accurate attenuation correction of emission data and electronic collimation that provide higher efficiency, more counts, and better statistics, all of which are the basis for better spatial and contrast resolution than single-photon systems.

A positron camera has four components: the scintillation detector-photomultiplier tube (PMT) modules, the gantry housing these detectors with its patient pallet, the electronics, and the computer systems. The design of each of these compounds and how they interrelate is essential for diagnostic accuracy, patient volume throughput, and for using ultrashort half-life, generator-produced ^{82}Rb for routine clinical studies without the expense of a cyclotron. Specific essential design features of a PET scanner for optimal clinical performance with ^{82}Rb are outlined below.

Generically, PET cameras contain 1000–1500 detectors in 3–8 banks of rings, attached to PMTs in ratios ranging from 1 to 8 detectors for each PMT. Scintillations from the coincidence detectors cause electronic signals from the PMTs that are converted to digital information and processed in a computer to reconstruct a tomographic image like a CT scan. However, the source of radiation is from a positron tracer, not an external x-ray tube. In order to optimize spatial sampling, the banks of detectors are wobbled in an eccentric path around the subject with each coincidence decay assigned a spatial location in the wobble path. A transmission image for attenuation correction is obtained by placing a ring of activity around the patient for imaging the target organ before injection of radiotracer. The positron radiotracer is then injected intravenously and an emission image obtained by back-projection techniques. The emission image is corrected for attenuation loss, random coincidences, scattered radiation, dead-time losses, wobble, and variation in detector sensitivity. A quantitative three-dimensional image of the radiotracer activity is obtained for the imaged organ.

Quantitative PET imaging refers to reconstruction of tomographic images that quantitatively reflect or recover the actual or true distribution of activity in the target organ or field of view undistorted by tissue attenuation, which is corrected by the transmission scan. This type of quantitative data recovery also depends on the technical characteristics of the camera and the duration of imaging permitted by the half-life of the positron tracer.

POSITRON-EMITTING RADIONUCLIDES (^{82}Rb)

Rubidium-86 was the first rubidium radiotracer used for coronary flow studies and therefore has the longest scientific history of all cardiac radiotracers (*22*). Subsequently, thallium-201 and technetium-99m were developed for single-photon imaging. Only relatively recently was cardiac PET in man first carried out with cyclotron-

produced ^{13}N-ammonia and [^{18}F]fluorodeoxyglucose (FDG). However, as with most mainstream technologic developments, these important initial radionuclides have been followed by a simpler, more economical, generator-produced tracer, ^{82}Rb. Rubidium radiotracers are analogs of potassium (and ^{201}Tl), the biologic behavior of which is more extensively described than any other cardiac radionuclide. For widespread, routine cardiac practice, a simple-to-use radionuclide source such as the ^{82}Rb generator is essential since it does not require a cyclotron (*23,24*) but allows all of the major aspects of cardiac imaging for clinical purposes as outlined below.

Rubidium is an alkali metal analog of potassium and is similar in chemical and biologic properties. It is rapidly concentrated by the myocardium with a first-pass extraction of 50%–60% at resting flow levels, which falls to 25%–30% at high coronary blood flows (*25–27*). By comparison, first-pass myocardial extraction of ^{13}N-ammonia is somewhat higher at 70%, falling to approximately 35% at high flows (*28–30*). With appropriately larger doses of ^{82}Rb (50 mCi), images are comparable to those of ^{13}N-ammonia (18 mCi) (*1*).

Because of its short half-life (75 sec), ^{82}Rb is the radionuclide of choice for repeated or sequential myocardial imaging. It is particularly useful in acute clinical situations in which the patient's condition is changing rapidly, or for studies before and after an intervention such as dipyridamole or PTCA.

Rubidium-82 is created from its parent, strontium-82, in a generator that uses hydrous SnO_2 as the inorganic absorbent. This generator has negligible ^{82}Sr breakthrough level, can be efficiently eluted with isotonic saline of physiologic pH, and delivers ^{82}Rb in a small eluate volume.

The use of short-lived, positron-emitting ^{82}Rb in cardiovascular nuclear medicine requires a system for rapid elution of an ^{82}Rb generator and on-line injection of the generator eluate. The ^{82}Rb infusion system incorporates features for efficient elution and precisely controlled delivery of a uniform, non-pulsating sterile solution of ^{82}Rb in saline. The system has preformed, sterile, disposable plastic tubing, one-way valves, and a syringe that are electromechanically-actuated to provide the eluent flow by positive flow pump action. The syringe plunger is bidirectionally actuated by a low-friction, recirculating ball screw jack that is coupled to a stepper motor through a reduction gear. The speed of the motor driving the syringe plunger and infusion rate is regulated automatically by a radiation monitor in line with the infusion tubing to deliver a predetermined dose and dose rate.

The components of the system—pump, fluid tubing, filters, one-way valves, electronic control modules, shielded vault for the ^{82}Rb generator, shield for the waste container, and dosimeter—are self-contained on a mobile cart. The elution and injection procedure is fully defined by the settings of the controls on the electronics modules for the infusion and dosimetry systems. Settings include eluted volume to be delivered, flow rate, dose to be delivered, dose rate, and patient volume to be delivered.

Comparison of ^{82}Rb and ^{13}N-ammonia

Rubidium-82 has several unique characteristics that are optimal for cardiac studies. Because of its short half-life, several sequential studies may be repeated at one sitting, such as before-and-after dipyridamole, PTCA, bypass surgery, drug therapy, episodes of acute ischemia, or serially following myocardial infarction. A rest-dipyridamole ^{82}Rb study requires 55 min compared with 2.50 hr for a study with cyclotron-produced ^{13}N-ammonia. Consequently, patient throughput is high with ^{82}Rb, demonstrated in private practice sites to be nine patients per day. With new attenuation correction methods that shorten the attenuation scan to 10 min (*31*), the time required for a rest-dipyridamole pair of scans is 40 min, thereby allowing 15 patient studies in a 10-hr shift. Since ^{82}Rb is generator-produced, it avoids the capital costs of a cyclotron and decreases the cost of radionuclide per study. Finally, ^{82}Rb provides data not only on myocardial perfusion but also on myocardial necrosis and viability simultaneously by processing the images in different ways during a rest-dipyridamole study (*1*). Thus, a rest-dipyridamole-viability study with ^{82}Rb requires only 55 min compared with 4–5 hr for obtaining comparable data with cyclotron-produced ^{13}N-ammonia and FDG.

CLINICAL SUMMARY OF CARDIAC POSITRON EMISSION TOMOGRAPHY

Clinical and experimental studies currently supporting the clinical applications for cardiac PET are listed below (*1*).

1. *Noninvasive Diagnosis of CAD in Either Symptomatic or Asymptomatic Patients.* The sensitivity and specificity of diagnosing CAD by PET (*1,32–39*) compared with automated quantitative coronary arteriography are both 95%–98% in symptomatic or asymptomatic individuals, including "balanced" three-vessel disease (*40,41*). False-negative studies are usually associated with distal coronary stenosis or disease of smaller arteries; false-positives are usually associated with nonatheromatous coronary artery abnormalities such as spasm or thrombi (*1,32, 35*). Table 1 lists the major studies from five different centers showing the accuracy of PET perfusion imaging. This application as compared with SPECT is discussed in more detail subsequently.
2. *Assessment of the Physiologic Severity of Coronary Artery Stenosis or Changes in Stenosis Severity.* As previously reviewed (*1*), percent diameter narrowing is not an adequate standard for quantifying stenosis severity of coronary artery narrowing (*1,32–35,40–50*), as also confirmed by others (*51–54*). Percent stenosis does not account for the effects of diffuse

TABLE 1
Updated Sensitivity and Specificity

Diagnostic test	Accuracy		Patients	Reference
	Sn	*Sp*		
Diagnosis of CAD artery disease by thallium stress testing since 1983	83%	47%	197	Van Train (107)
	85%	52%	1096	Ranhosky (108)
	95%	71%	210	DePasquale (106)
	76%	49%	832	Schwartz (113)
	82%	62%	461	Iskandrian (109)
	94%	52%	81	Bungo (114)
	94%	44%	242	Van Train (111)
Average weighted for #cases	84%	53%		
	67.5%	75%	"Corrected"	Diamond (118)
	65%	65%	"Corrected"	Gould (116, 117)
Diagnosis of coronary artery stenosis using ^{82}Rb with a fast PET scanner or $^{13}NH_3$	95%	100%	50	Gould (32)
	94%	95%	193	Demer (35)
	97%	100%	32	Schelbert (36)
	97%	100%	49	Yonekura (37)
	98%	93%	146	Williams (119)
Average weighted for #cases	96%	96%		

disease, eccentricity, stenosis length, absolute cross-sectional area, entrance and exit shape on flow, or flow capacity. It is also limited by substantial inter- and intraobserver variability. Alternative invasive approaches providing fluid dynamically correct measurements of graded stenosis severity utilize quantitative arteriographic methods to calculate stenosis resistance (*51*), pressure-flow curves (*49,50*), or coronary flow reserve (*32–43*).

The quantitative severity of PET perfusion defects after dipyridamole reflect the anatomic severity of the coronary artery stenosis as determined by automated, quantitative coronary arteriography, taking into account length, absolute dimensions, shape, and percent narrowing of the stenosis (*1,32–35,40–43*). Therefore, noninvasive positron emission tomography provides assessment of the physiologic severity of coronary stenosis as well as changes in severity after an intervention such as thrombolysis (*55*), bypass surgery (*56,57*), PTCA (*58*), or risk factor modification (*1,59,60*). With accurate quantitation of stenosis severity, binary classification of coronary artery disease based on sensitivity and specificity becomes inadequate or misleading for validating or describing diagnostic accuracy. This is one of PET's unique strengths, demonstrable by comparison to an appropriate arteriographic gold standard that takes into account all stenosis dimensions. Comparison of two noninvasive methods, e.g., PET versus SPECT, using arteriographic percent diameter stenosis as the standard, simply cannot be done because percent stenosis has little relation to coronary flow reserve (*32–35,40–43,52–54*) except for very severe narrowing. By definition, degrading quantitative data into a binary classification is necessarily incorrect because the inherent quantitative characteristics of the data are eliminated by the arbitrary binary classification analysis. Therefore, analyzing PET data according to a binary classification based on percent stenosis degrades the PET data to a nonquantitative status. Current literature does not report a quantitative relation of SPECT to stenosis severity by quantitative arteriography.

3. *Imaging Myocardial Ischemia, Infarction, and Viability.* The location and extent of myocardial infarction (*55–57,61–70*) and myocardial ischemia or viability (*44,55–57,61–71*) may be imaged by positron emission tomography with or without reperfusion using generator-produced ^{82}Rb or cyclotron-produced ^{13}N-ammonia and [^{18}F]FDG in order to determine if bypass surgery or PTCA is indicated. This application has been recently reviewed (*1*) as summarized subsequently.
4. *Identification and Assessment of Significant Collateral Function in Man by Imaging Coronary Steal During Dipyridamole-Handgrip.* Coronary steal occurs under conditions of near-maximum coronary vasodilation if collaterals provide a significant proportion of resting myocardial perfusion. A fall in absolute myocardial activity after injection of a perfusion tracer during dipyridamole vasodilation compared with rest indicates coronary steal and the presence of significant collaterals (*72–74*). Because it is physiologically complex and uniquely assessed by PET, myocardial steal is addressed in more detail elsewhere (*1*).

5. *Dilated Cardiomyopathy.* This condition is unrelated to CAD and may also be diagnosed by positron imaging as an enlarged, poorly functioning heart with no resting or stress perfusion defects typical of ischemic cardiomyopathy due to coronary artery disease.
6. *Left Ventricular Function and Wall Thickening.* By gating the positron-emission tomographs with the ECG, left ventricular pumping function and wall thickening may be assessed regionally in three dimensions (*32,75*). Since there are many other less expensive, simpler measures of left ventricular function, gated PET has not been developed clinically. However, since PET is recognized as a noninvasive substitute for diagnostic catheterization, recording first-pass gated blood-pool for LV function as a part of routine perfusion studies will likely become a common method to obtain complete cardiac evaluation comparable to catheterization for the basic questions of arterial patency, myocardial viability, stress underperfusion, and left ventricular function.

PHYSIOLOGIC PRINCIPLES OF PET PERFUSION IMAGING

With marked increases in coronary flow, functionally mild, early coronary artery stenosis can be identified before symptoms of myocardial infarction occur, thereby allowing medical therapy aimed at reversal of coronary atherosclerosis. However, with only modest increases in coronary flow as during exercise stress, only severe coronary stenoses can be identified. An inadequate stimulus for increasing coronary flow or an inadequate perfusion imaging agent or technique will limit the ability to detect or quantify coronary stenosis by perfusion imaging. Based on animal studies (*40,45–50,76*) and confirmed in man (*1,32,35,47, 48*), there are three essential principles of an imaging method for detecting and assessing severity of coronary artery disease: (a) cross-sectional PET to avoid overlapping structures and to obtain depth-independent resolution for accurate quantitative images of coronary blood flow; (b) a myocardial perfusion imaging agent taken up or deposited in myocardium in proportion to flow at high coronary blood flows up to five times resting control levels; and (c) a potent stimulus for increasing coronary flow to image the regional disparities in maximum perfusion caused by stenosis. Figure 1 demonstrates these principles. In the top panel, resting coronary flow and distribution are normal despite a severe stenosis. After i.v. dipyridamole, flow increases four times base-line (middle panel) in the normal area but is restricted to a two times increase in the diseased area. There must be an average ratio of 2.4:1 or 150% difference between normal and affected areas to visibly detect a relative perfusion defect on planar thallium image in experimental animals. With PET, a difference of only 15% can be detected, i.e., an abnormal area that is 85% of normal maximum. This capacity makes PET the most sensitive and specific nuclear cardiology procedure for coronary atherosclerosis.

The ratio of radionuclide activity after dipyridamole to activity at rest reflects absolute flow reserve. The ratio of activity in a perfusion defect to normal maximum activity in distribution of normal coronary arteries on the dipyridamole image reflects relative coronary flow reserve. With quantitation of PET perfusion imaging to account for arterial input function and flow-dependent radionuclide extraction, absolute and relative coronary flow reserve may be quantitatively measured by PET (*40*).

Absolute and Relative Coronary Flow Reserve

The concept of coronary flow reserve, defined as maximum flow divided (normalized) by resting control flow, has evolved into an accepted functional measure of stenosis severity since first proposed by Gould (*77–80*). Its validity has been confirmed and applied clinically by noninvasive imaging (*1,32–36,40,45–50,76–89*) and by invasive methods such as coronary sinus thermodilution (*90*), Doppler-tip catheters (*91–93*), and digital subtraction angiography (*94,95*). These clinical methods measure pharmacologically-induced increases in coronary blood flow, most commonly with i.v. dipyridamole for noninvasive studies and intracoronary papaverine for invasive studies.

Coronary flow reserve has also been integrated theoretically with, and experimentally related to, the geometric

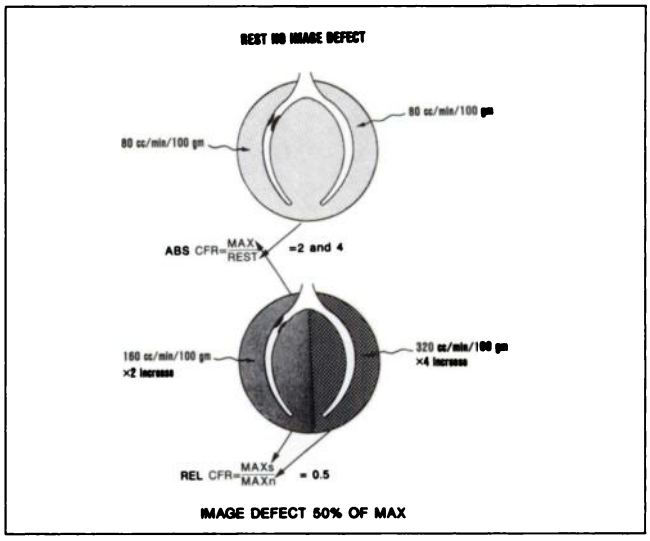

FIGURE 1. Schema demonstrating the principle for detection of coronary artery disease by perfusion imaging under conditions of maximum coronary vasodilation. With an 80% diameter narrowing, coronary flow reserve is limited to approximately a two times increase over resting levels as compared to a four times the increase in non-stenotic arteries. The abnormal area, therefore, has 50% less activity, reflecting a 50% decrease in maximum flow compared to normal maximum. ABS CFR is absolute coronary flow reserve and REL CFR is relative coronary flow reserve.

dimensions of stenosis (*32–35,40,82–84*). The commonly used percent diameter stenosis is poorly related to functional severity of human coronary artery narrowing or coronary flow reserve (*32–35,40,52–54,82–84,92–96*), determined by quantitative coronary arteriography as in Figure 2 (*35*) or by directly measured flow reserve using a Doppler catheter (*93*). Thus, extensive experimental and clinical literature have substantiated the concept of coronary flow reserve.

However, changes in aortic pressure and heart rate are known to alter cardiac workload and therefore baseline coronary blood flow as well as altering maximum coronary flow under conditions of maximal vasodilation (*40*). Consequently, *absolute coronary flow reserve*, as measured by flowmeter, also varies with aortic pressure and heart rate independent of stenosis geometry due to differential effects of these variables on resting and maximal coronary flow. Under markedly varying physiologic conditions, or from patient to patient, absolute coronary flow reserve may not reliably or specifically reflect severity of coronary artery narrowing since it may be altered by physiologic factors unrelated to stenosis geometry.

In contrast, relative maximum coronary flow or relative flow reserve, defined as maximum flow in a stenotic artery divided (normalized) by the normal maximum flow in the absence of stenosis, should theoretically be more independent of aortic pressure, heart rate, or varying baseline flow caused by changing cardiac workload. Physiological variables unrelated to stenosis severity, such as aortic pressure, heart rate, metabolic demand, or vasomotor tone, alter distal coronary bed resistance in series with, and independent of, proximal stenosis resistance. During maximal coronary vasodilation, distal coronary bed resistance is equally minimized for both normal and stenotic arteries. When the maximum flow in the stenotic artery is normalized by normal maximum flow, the term for minimum bed resistance reflecting effects of pressure, (heart rate or vasomotor tone on flow in the numerator and denominator of this ratio) are cancelled (*40*). Therefore, relative differences in regional maximum flow, or relative flow reserve, are determined primarily by geometric genetic stenosis severity. Relative flow reserve is therefore a measure of stenosis severity independent of physiologic variables.

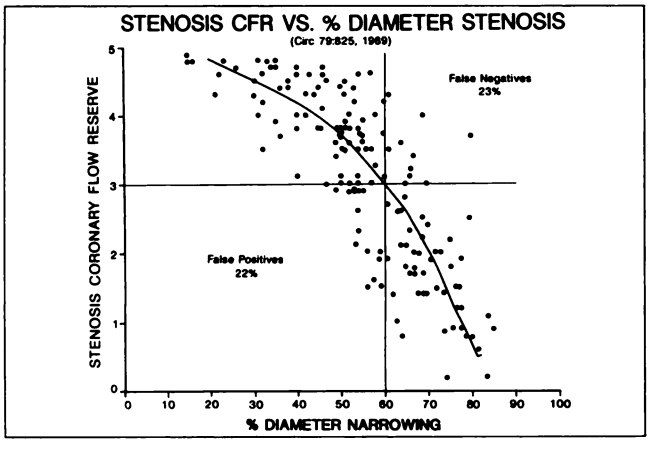

FIGURE 2. Graph of the relation between stenosis flow reserve and percent diameter narrowing, both determined from automated quantitative arteriographic measurements in 100 patients. Because percent diameter narrowing is only one of several factors used to calculate stenosis flow reserve, the scatter in this relation indicates the importance of those factors other than percent stenosis that influence flow impedance of a stenosis. Reproduced with permission from reference (*35*).

Rather than considering absolute coronary flow reserve to be competitive or antithetical to relative flow reserve, our data indicate that these measurements are independent variables providing complementary information. Absolute flow reserve is the flow capacity of the stenotic coronary artery and vascular bed under any conditions of pressure, workload, hypertrophy, vasomotor tone, or stenosis. It reflects the cumulative effects of these various factors without being specific for the mechanism or cause of altered flow reserve. Relative coronary flow reserve reflects more specifically the effects of the stenosis independent of and unaffected by the other physiologic variables if normal maximum flow is high enough. Thus, absolute and relative coronary flow reserve are complementary.

"Balanced" three-vessel coronary artery disease may theoretically cause a false-negative stress perfusion test depending upon the stress stimulus and the imaging technology, particularly in spatial and contrast resolution. Based on our experience with PET, most hearts affected by CAD contain some unaffected artery that serves as a reference area. However, small-vessel disease, left ventricular hypertrophy, or theoretically "balanced" three-vessel coronary artery disease are potential causes of diffusely impaired flow reserve that must be accounted for in individual patients. For this purpose, some measure of absolute as well as relative coronary flow reserve is necessary. However, relative flow reserve is also necessary since it is not affected by variability in pressure or heart rate within the same patient or among patients.

Clinical Implications of Absolute and Relative Flow Reserve

A stress myocardial perfusion image shows relative maximum perfusion (radiotracer uptake) or relative coronary flow reserve. One of the purported limitations of radionuclide perfusion imaging is its inability to measure absolute flow and absolute coronary flow reserve. However, perfusion imaging of relative maximal coronary flow or relative flow reserve has been useful for assessing physiologic stenosis severity, despite greatly changing or widely variant physiological conditions seen between rest conditions and upright treadmill exercise, bicycle stress, supine exercise, or various pharmacologic stresses such as dipyridamole and papaverine. The results of our study explain this observation. The stress perfusion image shows relative coronary flow reserve, which is independent of physiologic variables of blood pressure and heart rate. Thus, what has

long been considered the limitation of stress perfusion techniques is in fact its greatest advantage.

In order to be optimally effective over the wide range of conditions seen clinically, a method for assessing physiologic stenosis severity should provide measures of both relative and absolute flow reserve. For example, measurement of absolute flow reserve in a coronary artery by a Doppler-tip catheter after adenosine or papaverine indicates the effects of single-, multiple-vessel, or diffuse CAD. However, this may change somewhat due to markedly varying afterload and baseline pressure-rate product or physiological differences among patients that affect flow reserve separate from stenosis geometry. On the other hand, relative coronary flow reserve, as assessed by current standard thallium perfusion imaging, does not adequately reflect the absolute flow response to vasodilator stimuli or diffuse atherosclerosis affecting all coronary arteries. Most invasive or noninvasive clinical methods as now used provide measurements of either absolute or relative coronary flow reserve, but not both, with the exception of positron emission tomography.

Therefore, the optimal noninvasive method uses relative coronary flow reserve to assess physiologic stenosis severity and absolute flow reserve to assess response to dipyridamole, small-vessel disease, left ventricular hypertrophy and "balanced" three-vessel disease, as well as single or multiple coronary artery stenosis of varying severity.

Absolute and relative coronary flow reserve are independent, complementary variables, which together more completely describe physiologic severity of coronary artery narrowing than either alone. These conclusions have important implications for clinically assessing physiologic stenosis severity by noninvasive perfusion imaging using positron emission tomography.

Finally, Figure 2 also shows why a single threshold percent diameter stenosis is a poor gold standard of disease severity for comparison to perfusion imaging. For a hypothetically perfect imaging technique that measured coronary flow reserve exactly as by a flowmeter, false-positive and false-negative tests would be 22% and 23% for a threshold of 60% diameter stenosis. Thus, perfect physiologic measures of coronary flow reserve would appear diagnostically poor with a sensitivity and specificity of 77% and 78%, due to the inadequacy of using a percent stenosis threshold as a gold standard of significant disease.

INDICATIONS FOR CARDIAC PET BY DIAGNOSTIC CATEGORY

Examples of Physiologic Diagnosis by PET

Angina Pectoris. Assessing severity, extent, location of coronary artery stenosis, and status of collaterals. Figure 3 shows rest-dipyridamole PET of generator-produced ^{82}Rb in a 61-yr-old man with angina pectoris needing evaluation for severity/extent of disease and for following regression or progression of coronary artery disease.

True short axis views are shown in Figure 3A; horizontal and vertical long axis views are shown in Figure 3B (*41*). Rest images are uppermost in each pair of image rows (study 1). The dipyridamole images are in the lower row of each pair of image rows (study 2). The number after the decimal is the image plane for both studies 1 and 2. In the color coding, white indicates the highest flow, red next highest, yellow intermediate, and green and blue the lowest relative flows. The tomographs in the horizontal long axis views (top images of panel 3B) are oriented as if looking down from above with anterior or apex at the top of each image, left lateral free wall on the left, and muscular septum on the right with AV ring and/or inferior myocardium at the bottom. In true short axis views of panel 3A the image planes are arranged from the AV ring at the upper left to the apex at the lower right with anterior wall being up, free LV wall on the left, and septum on the right of each tomograph. The open "C"s in the basal short axis views in the upper left images of Figure 3A are caused by the membranous septum of the LV cavity, which is avascular and therefore appears as a defect but reflects normal anatomy.

The resting tomographs show a small apical defect indicating a small myocardial scar. With dipyridamole the anterior, septal, and apical myocardium show a defect in both short and long axis views. The inferior and lateral myocardium do not show a definite stress perfusion defect on tomographic views. However, the entire set of data analyzed together on the polar coordinate maps suggests abnormal relative flow reserve (lower left polar coordinate map) and absolute flow reserve (right upper polar map in the bottom half of the image).

Figure 3B shows horizontal (left) and vertical (right) long-axis views of the heart. Rest images are shown in the top row with dipyridamole stress images in the lower row of the top half of the figure. The horizontal long axis views are oriented as if looking down from above. The vertical long-axis tomographs are oriented as if looking at the left side of the body cut head to toe; anterior myocardium at the top, inferior at the bottom, apex at the left, and AV ring on the right.

Tomographic data are summarized in a polar display as if looking at the patient from the outside toward the LV apex located in the center of the bull's-eye with the outer rim of the bull's-eye corresponding to the AV ring. Polar displays on the left (lower half of figure) show the relative activity on a scale of 0% to 100% with rest being the upper (S1) and dipyridamole stress being the lower (S2) of the polar maps on the left side of the panel. The upper right polar map (in the lower half of the figure), labeled absolute S2/S1 ratio (ABS S2/S1), shows the absolute counts of stress image divided by rest image, displayed on a scale from 0 to 2, reflecting absolute coronary flow reserve.

Increase in activity on a dipyridamole image compared with rest is shown by warm colors (yellow, orange, red, white) indicating ratios greater than one (blue), which

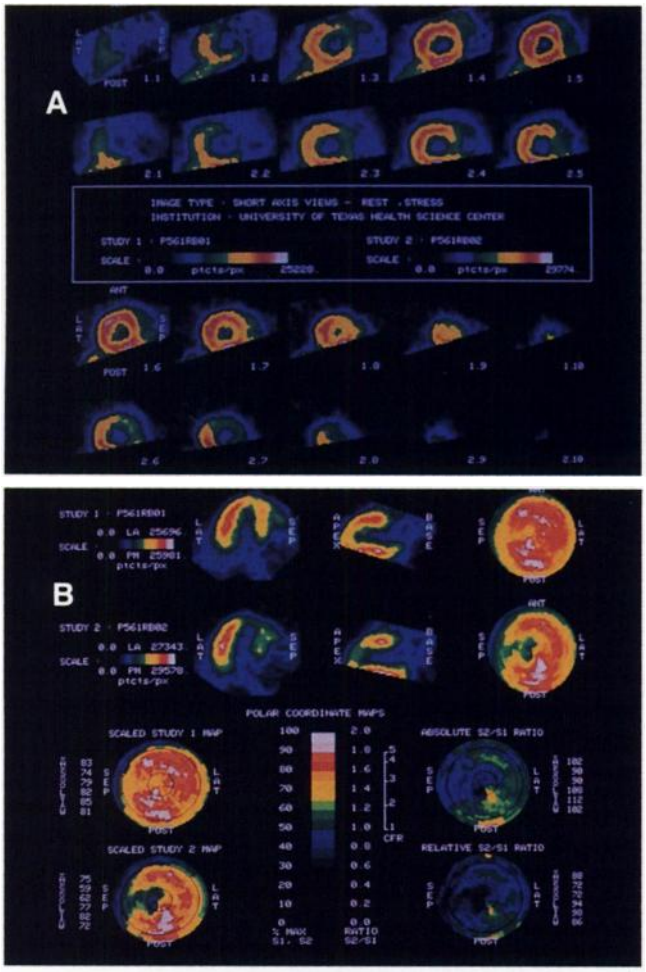

FIGURE 3. Rest-dipyridamole PET images using ^{82}Rb of a patient with three-vessel coronary artery disease. See text for details of the display, which are identified here as follows.
(A) Short-axis views. The upper row of each pair is rest and the lower row is the dipyridamole image set.
(B) Horizontal and vertical long-axis views with polar map displays of minimum activity in each quadrant and whole heart.
(C)Three-dimensional topographic displays of the heart in septal, anterior, lateral, and inferior views (see text for details). Reproduced with permission from references (*1*) and (*41*).

reflect increased radiotracer uptake and perfusion due to dipyridamole. Beside the scale for absolute S2/S1 radiotracer uptake ratio (stress/rest) is a scale of coronary flow reserve values derived by a two-compartment model accounting for flow-dependent extraction derived from animal studies. The lower right polar display, labeled relative S2/S1 ratio (REL S2/S1), shows the relative distribution of flow after dipyridamole divided by the relative distribution of activity on the rest image (relative instead of absolute values), also on a scale from 0 to 2. It therefore maps the relative change in activity from rest to stress.

Letters and numbers beside each polar map show quantitative results. For regions of the heart, A = anterior, S = septal, X = apex, L = lateral, I = inferior. The numbers beside each region indicate the minimum activity as a percent of normal areas (100%). For letters with a bar, i.e., $\bar{A}$, the numbers indicate mean activity of all pixels (rather than minimum) for that quadrant of the polar map as percent of normal areas (100%).

In the example in Figure 3B, visual inspection of the polar map display and quantitative analysis show considerably more information than obtained from visual inspection of the tomographic views alone. The polar map S2 of relative flow reserve shows not only a severe decrease in relative activity of the anterior, septal, and apical areas, but also a mild decrease in the inferior septal area not apparent on tomographic views but confirmed by the minimum activity decreasing on S2 (stress) compared with S1 (rest). The lateral wall also shows a visual and quantitative decrease in activity reflecting a mild relative decrease throughout the lateral quadrant not apparent on the tomographic views. On the polar map on the upper right (Fig. 3B), absolute S2/S1 ratio shows that at least one part of the heart located inferior-laterally responded with a flow reserve of 2.8 (times baseline). Flow reserve in the rest of the heart was severely depressed, indicating three-vessel disease with the LAD proximal to the first septal perforator being most severely affected, and disease of the left circumflex and right coronary arteries. The relative flow reserve defect on S2 is not as apparent as the marked defect of absolute flow reserve on S2/S1, consistent with the discussion of the previous chapter.

In addition, parts of the anterior septum and apex show a decrease in absolute counts with an absolute ratio of less than one on the absolute S2/S1 ratio polar map. A fall in absolute activity after dipyridamole compared with rest indicates myocardial steal and hence the presence of collaterals to viable myocardium. On the S2/S1 absolute ratio

polar map, a large part of the whole myocardium shows myocardial steal and is therefore viable, collateralized myocardium, mostly in the anterior, septal, and apical regions. Thus, the location, intensity, size, statistical significance, and presence of collateralized viable myocardium can be automatically quantitated.

In addition to standard tomographs and polar maps, new three-dimensional (3-D) topographic displays of cardiac PET are shown in Figure 3C. These 3-D topographic displays do not distort the spatial size and shape of defects as do polar map displays. They therefore provide more accurate spatial quantitation and visualization of abnormalities compared with previously shown polar maps (*1*). Three-dimensional topographic maps of cardiac PET images are derived from short-axis data. Each panel of the topographic map views the left ventricle as if looking at the septum (first panel), the anterior wall (second panel), the left lateral wall (third panel), or the inferior wall (fourth panel). The rest study is shown in the upper row (S1) and the stress study in the lower row (S2). The dashed white line marks the upper limit of automated quantitative data since the membranous septum often causes a normal defect at the AV ring. The black dashed lines delineate septal, anterior, lateral, and inferior quadrants with the lower dashed line delineating the apex. The colored scaling and automated quantitation, such as minimum activity values, mean activity in each quadrant, and percent of myocardium beyond 1.5, 2.0, and 2.5 standard deviations are all the same as previously described for polar maps.

The rest 3-D topographic display (Fig. 3C) showed a mild small apical defect suggesting a small apical scar. The dipyridamole scan showed severe defects of large size in the anterior, septal, apical, anterior lateral, lateral, posterior, and inferior myocardium (*1*). A small segment of inferior lateral myocardium demonstrated increased uptake of tracer indicating response to dipyridamole.

An extensive area, approximately one-third of myocardium in anterior, apical, and inferior apical distributions, demonstrated decrease in activity during dipyridamole compared with rest, suggesting myocardial steal and collateralization. These images were interpreted as showing occlusion of the LAD and right coronary arteries as commonly seen with such extensive resting collateral flow and a tight stenosis of the left circumflex coronary artery. Coronary arteriography confirmed these findings, demonstrating complete occlusion of the proximal LAD and right coronary arteries, which were supplied extensively by collaterals from smaller proximal branches of these arteries as well as from the left circumflex.

Asymptomatic Patient with Hypercholesterolemia. In order to further illustrate the application of clinically assessing both absolute and relative coronary flow reserve, Figure 4 shows an example of a PET study at rest and after dipyridamole stress using generator-produced ^{82}Rb in an asymptomatic man with no known cardiac disease or events who had hypercholesterolemia and a normal thallium treadmill test (*40*). The short-axis rest-dipyridamole views (Fig. 4A) are normal. The polar map of dipyridamole study (4B, S2, lower left polar map) reflects regional relative coronary flow reserve on the same scale of 0%–100% and is abnormal. Every quadrant in the dipyridamole polar map shows a fall in relative minimum intensity from 82% to 73% of normal in the anterior (A) quadrant, from 73% to 65% in the septal (S) quadrant, from 68% to 50% in the apex (X), and from 74% to 67% in the inferior quadrant with the high lateral quadrant showing no relative defects, 67% to 66%. However, the relative flow reserve image, S2, does not show a localized regional or sharply circumscribed relative flow reserve defect.

The upper right polar map labeled ABS S2/S1 shows the absolute activity in the stress study (S2) divided by the absolute activity in the rest study (S1) expressed as absolute coronary flow reserve using a model accounting for radionuclide extraction, dose, and cardiac output changes. In this instance, the maximum regional coronary flow reserve located in the anterior-lateral area of the heart in response to dipyridamole was 4.0 (times resting levels), indicating that this patient responded well to dipyridamole in a small artery to the high anterior lateral myocardium. Since flow reserve was reduced to every quadrant of the heart except to this high anterior lateral area, the PET scan was interpreted as showing mild to moderate "balanced" three-vessel disease without knowledge of clinical data or arteriograms. Thus, despite "balanced" three-vessel disease affecting all major arteries of the heart, at least some part of the myocardium responded well to this vasodilator stimulus as a normal reference area. By using measures of both relative and absolute coronary flow reserve, "balanced" three-vessel disease was identified. Coronary arteriography confirmed 50%–60% diameter narrowing of the three major coronary arteries. This patient began vigorous dietary and pharmacologic cholesterol lowering that would not have been otherwise started without a PET study. Corresponding 3-D topographic displays in Figure 4C show the rest scan in the upper row (S1) and dipyridamole scan in the lower row (S2), demonstrating mild defects of septal, anterior, apical, lateral, and inferior areas.

Atypical Chest Pain. The patient was a 53-yr-old man with 20 yr of nonexertional chest wall pain believed to be caused by cervical root compression. He had a normal thallium and ECG treadmill test 1 yr and 10 days prior to PET scan. His rest PET study is shown in the upper row (S1) and dipyridamole study in the lower row (S2) in long axis and polar map displays in Figure 5A (*1*). Three-dimensional topographic maps are shown in Figure 5B. Each panel of the topographic map (Fig. 5B) views the left ventricle as if looking at the septum (first panel), the anterior wall (second panel), the left lateral wall (third panel), or the inferior wall (fourth panel).

In Figures 5A-B, the rest image (upper row) showed a mild small apical defect, suggesting a small, old, apical myocardial infarction despite absence of a clinical event.

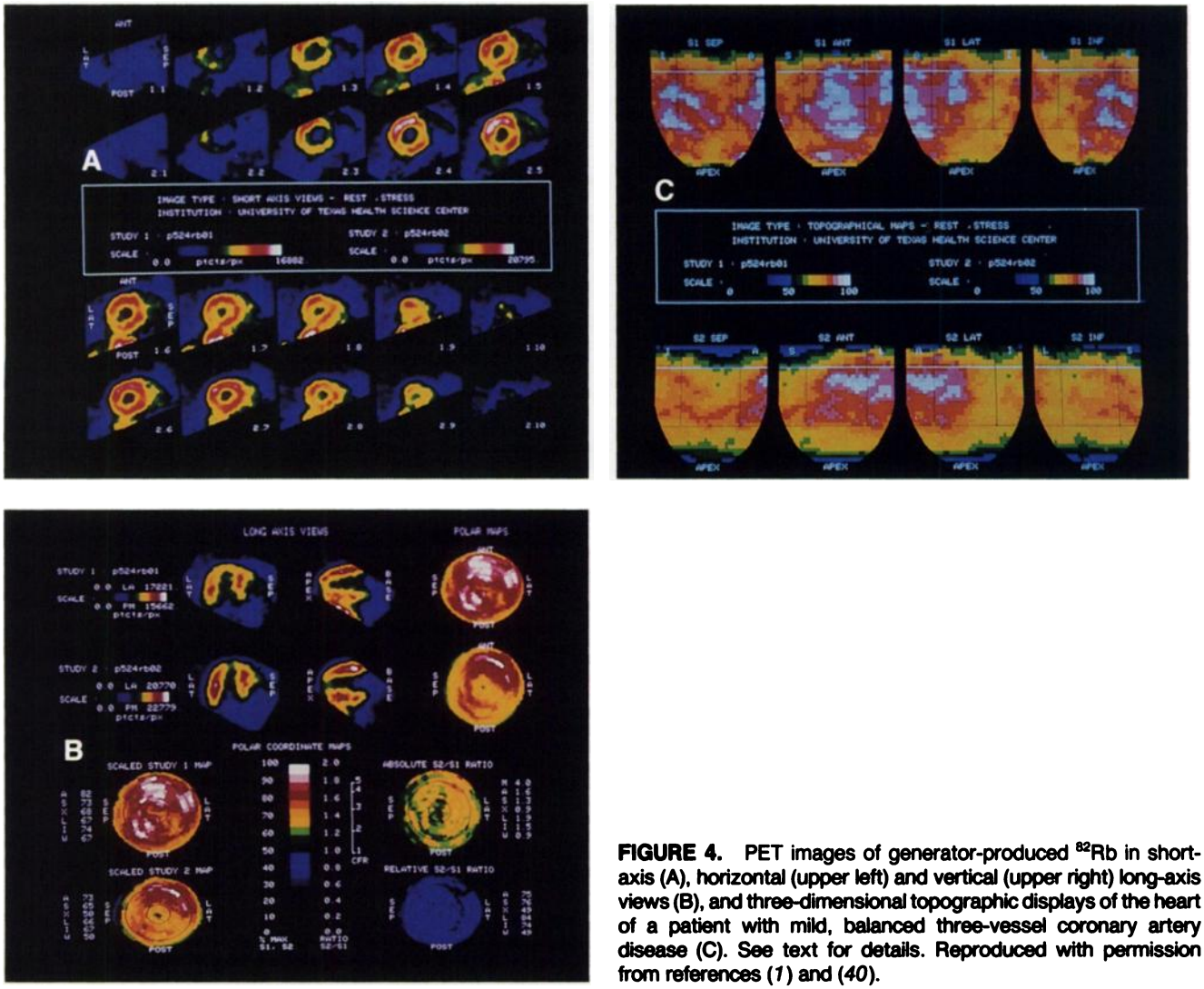

FIGURE 4. PET images of generator-produced ^{82}Rb in short-axis (A), horizontal (upper left) and vertical (upper right) long-axis views (B), and three-dimensional topographic displays of the heart of a patient with mild, balanced three-vessel coronary artery disease (C). See text for details. Reproduced with permission from references (*1*) and (*40*).

The dipyridamole image (lower row) showed a large severe anterior and apical defect involving 29% of myocardium outside 2.5 standard deviations from normal. There were definite but less severe defect of the anterior septum and lateral wall. These results were interpreted as showing a very severe mid-LAD, another more moderate severe LAD stenosis proximal to the first septal perforator, and a moderate stenosis of an artery to the lateral myocardial wall, probably a left circumflex stenosis. Left ventricular function was normal.

Accordingly, the patient was scheduled for diagnostic catheterization and PTCA of three lesions with surgical backup. Quantitative coronary arteriography confirmed significant stenosis of the proximal and mid-LAD, and the mid-left circumflex. PTCA was carried out on these three lesions due to severity of the disease involving a large extent of myocardium.

Following CAD in Asymptomatic Patient. The patient was a 61-yr-old white male who had a previous inferior myocardial infarction, sudden death with successful resuscitation, and recurrent inducible ventricular tachycardia controlled on drugs. He had never had chest pain or other symptoms and had no physical limitations. Coronary arteriography showed an occluded right coronary artery filling distally through collaterals, an occluded diagonal, a 50% diameter stenosis of the obtuse marginal, a 50% diameter stenosis of the proximal LAD, and no segmental narrowing of the left circumflex coronary artery. PET scans showed a fixed inferior defect without perfusion abnormalities anterior or laterally (not shown).

Since the patient had never had angina pectoris as an end point for following his disease, which presented with myocardial infarction/sudden death, routine follow-up PET scan was obtained 6 mos later without symptoms or change in his clinical status. The rest scan was unchanged from the previous study showing inferior scar. In Figure 6 (*1*), comparison of the first stress scan (upper row, S1) with the follow-up stress scan (lower row, S2) showed a new moderate mid-anterior wall perfusion defect and a severe lateral perfusion defect not present previously. The routine follow-up PET scans therefore demonstrated moderate progression of the mid-LAD lesion and appearance

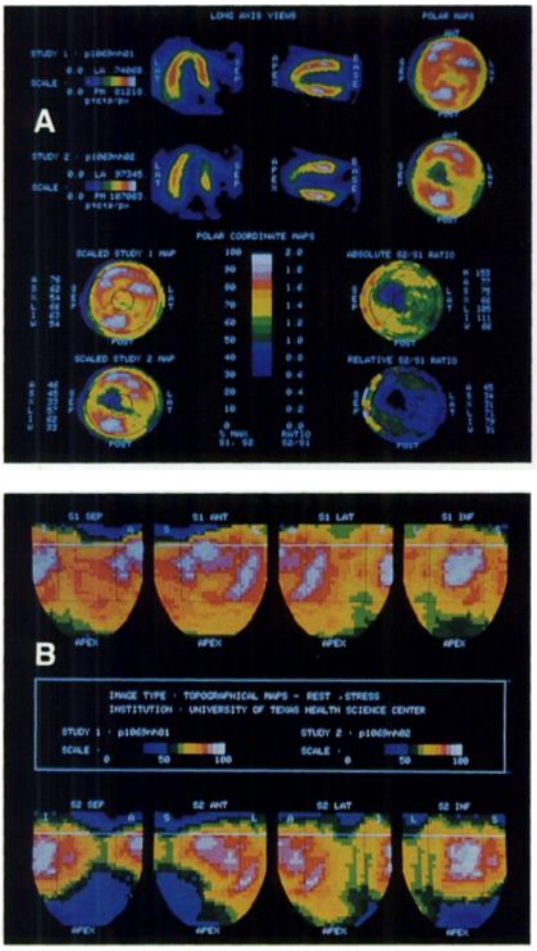

FIGURE 5. PET images in long-axis views and polar maps (A) and three-dimensional topographic displays of (B) a patient with two normal thallium/ECG stress tests. See text for details. Reproduced with permission from reference (*1*).

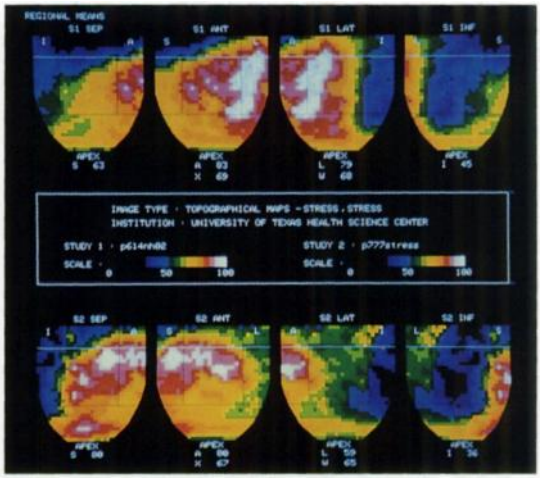

FIGURE 6. PET images in three-dimensional topographic displays showing the first stress study (upper row) and a second stress study 6 mo later (lower row). See text for details. Reproduced with permission from reference (*1*).

of a new, severe defect in the left circumflex distribution not present previously.

Repeat coronary arteriography confirmed progression of the mid-LAD stenosis from 50% to 70%. The left circumflex, which previously had not demonstrated significant localized narrowing, had developed a 90% stenosis in its proximal portion. As a result of PET findings, the patient was sent to bypass surgery since symptoms were an inadequate guide to progression of this disease.

REVERSAL OF CORONARY ARTERY STENOSIS

The question often arises whether accurate detection of coronary atherosclerosis is clinically useful, particularly in asymptomatic subjects. Although overwhelming epidemiologic evidence links coronary heart disease to smoking, serum cholesterol, hypertension, and family history, large trials of modest risk factor modification with mortality end points have been somewhat disappointing, as recently reviewed (*1*). In contrast with these previous large clinical trials, the randomized arteriographic trial of Ornish and Gould (*1,59,60*), the CLAS study by Blankenhorn et al. (*97*), and the FATS trial by Brown et al. (*98*) demonstrate that reversal of coronary artery stenosis in man is feasible.

The Ornish-Gould study was the first randomized, controlled, blinded, arteriographic trial to determine the effects of strict risk factor modification on the geometric dimensions, shape, and fluid dynamic characteristics of arteriographic coronary artery stenosis in man (*1,59,60*). Using percent diameter stenosis as the end point that is the most widely recognized measure of stenosis severity, this study demonstrated regression or cessation of progression in approximately 80%–85% of treated patients compared to approximately 80%–85% progression in the control group. Brown et al. (*98*) also demonstrated cessation of progression or reversal of percent stenosis in patients with diet and multiple cholesterol-lowering drugs, as well as a dramatic decrease in myocardial infarction, sudden death, and bypass surgery/PTCA in the treated versus control group.

However, complex changes of different stenosis dimensions in opposite directions or to different degrees may cause stenosis shape change with profound effects on fluid dynamic severity unaccounted for by simple percent narrowing. Accordingly, we analyzed all stenosis dimensions on coronary arteriograms including absolute proximal, minimal, distal lumen diameter (area), percent stenosis, integrated length, and exit effects to determine stenosis shape and a single integrated measure of functional severity and stenosis flow reserve, incorporating the fluid dynamic effects of all these dimensions (*1,59,60*). In the control group, complex shape change and stenosis molding characteristic of statistically significant progressing severity occurred with worsening of stenosis flow reserve. In the treated group, complex shape change and stenosis molding characteristic of significant regressing severity was observed with improved stenosis flow reserve (*1*). The improved geometry was associated with marked reduction in

angina pectoris such that at the end of the study, most patients in the treated group were off cardiac drugs. These results document for the first time the multidimensional characteristics of regressing coronary artery stenosis in man associated with risk factor modification.

However, only patients with known CAD require marked lifestyle change (*59,60*) or lowering of serum cholesterol with multiple drugs (*97,98*) to prevent progression or reverse severity of coronary artery stenosis. Such vigorous lifestyle change or drug interventions may not be appropriate for those individuals with risk factors who do not have coronary artery stenosis. Those individuals who do have coronary heart disease or a genetic predisposition to it need more aggressive risk factor interventions than are indicated for the general population or for those with modestly elevated cholesterol without coronary artery stenosis. While community education programs are important, their target guidelines for diet or drug therapy are not as stringent as necessary for a patient with documented CAD or a genetic predisposition. Therefore, the vigor of risk factor modification should increase with the probability or certainty of having CAD. Vigorous medical reversal therapy should also be considered as an additional step in patients undergoing mechanical intervention in so that progression of disease does not negate the benefits of mechanical intervention.

These observations have major implications for controlling health care costs of cardiovascular disease as discussed subsequently.

QUANTITATIVE CORONARY ARTERIOGRAPHIC GOLD STANDARDS

The sensitivity and specificity of diagnosing CAD by PET are both 95%–98% in symptomatic or asymptomatic individuals (*32–39*), including "balanced" three-vessel disease (*40,41*). False-negative studies are usually associated with distal coronary stenosis of moderate severity or disease of smaller arteries in which arterial bed size is small, minimizing the defect intensity or contrast between normal and abnormal areas. False-positives are usually associated with nonatheromatous coronary artery abnormalities such as spasm, thrombi, or myocardial muscle bridge. Although this diagnostic accuracy surpasses other noninvasive technologies for evaluating CAD, measuring diagnostic accuracy by the end points of sensitivity and specificity fails to account for the quantitative capacity of PET to assess severity and size of involved areas rather than just presence or absence of disease.

Most reports on the diagnostic accuracy of myocardial perfusion imaging have used sensitivity/specificity to describe the relation between perfusion image defects and arteriographically documented disease. This approach requires binary (positive or negative) classification of both imaging and arteriographic results. Perfusion images have been classified as normal/abnormal and arteriographic stenosis severity has usually been described in terms of a threshold percent diameter narrowing, such as 50% stenosis, as the criterion for presence of CAD.

There are three limitations to this use of sensitivity/specificity analysis for assessing accuracy of noninvasive tests for coronary disease. First, coronary atherosclerosis is not an all-or-none condition. Binary classification requires arbitrary threshold criteria and creates artificial classifications for a disease that has a continuous spectrum of severity by both arteriography and perfusion imaging. Threshold values that yield optimal sensitivity and specificity values for one test may yield optimal sensitivity and specificity values for one test may yield falsely lower values for a different but more accurate test if its detection threshold is different. For example, an imaging test capable of detecting 40% stenosis may have low specificity according to a 60% stenosis criterion but high specificity according to a 40% stenosis criterion. Second, sensitivity and specificity are markedly affected by disease severity and distribution in the study population (*99–101*). A sample population with a high frequency of mild disease will be distributed centrally near the threshold values where scatter is more likely to lower sensitivity and specificity. A sample population with a high prevalence of severe disease resulting in good contrast between normal and abnormal areas of an image will produce good sensitivity/specificity.

Thus, the sensitivity and specificity found in one population may not apply to a different population. The most severe test for a noninvasive method is a low-prevalence, asymptomatic population. In the University of Texas study (*35*), 40% of patients were asymptomatic, a much larger prevalence of asymptomatic individuals than previously reported for SPECT and therefore a more realistic test population for comparing PET and SPECT. In a subset of 46 patients with both PET and SPECT, for moderately severe disease with stenosis flow reserve of <3, PET detected 95%, whereas SPECT detected 58%; for a flow reserve of 3–4, PET detected 52% and SPECT detected none.

To overcome the limitations of sensitivity/specificity as end points of diagnostic effectiveness, an analysis of test results as continuous variables has been proposed; however, this requires quantitative analysis of PET scans and arteriography (*32–35,40–43,45–50,102*). In addition to these limitations, we have also shown that percent diameter narrowing is not an adequate standard for quantifying stenosis severity of coronary artery narrowing. Percent stenosis does not account for the effects of diffuse disease, eccentricity, stenosis length, absolute cross-sectional area, entrance and exit shape, and absolute dimensions on flow or flow capacity. It is limited by substantial inter- and intraobserver variability. Alternative approaches providing fluid dynamically correct measurements of graded stenosis severity utilize quantitative arteriographic methods to calculate stenosis resistance (*51*), pressure-flow curves (*49, 50*) or stenosis flow reserve (*32–35,40,50*).

Quantitative coronary arteriography predicts the func-

tional pressure-flow characteristics of stenosis directly measured by flowmeter if all the dimensions of the lesion are taken into account, including relative percent narrowing, absolute luminal area, shape, and integrated length effects (*32–35,40,49,50*). Because these multiple dimensions have cumulative hemodynamic effects and interact with each other, they are combined by fluid dynamic equations into a single measure of stenosis severity, which are applicable clinically to stenosis flow reserve. Stenosis flow reserve is the same as coronary flow reserve but instead of being measured directly by flowmeter, stenosis flow reserve is derived from all geometric dimensions of the narrowing as a standardized, single, integrated measure of its severity for standardized conditions of pressure and normal reference vasodilator reserve, as described elsewhere (*1*).

Thus, we use the term stenosis flow reserve in reference to calculated coronary flow reserve derived from anatomic stenosis dimensions by quantitative analysis of coronary arteriograms. We use the term coronary flow reserve for flow reserve directly measured by a flowmeter, Doppler catheter, or perfusion imaging. The concept of arteriographic stenosis flow reserve has been well developed theoretically, validated by comparison with directly measured flow reserve experimentally (*33,40*) and proven clinically valuable by comparison with regional PET perfusion defects in patients (*32,35*). Therefore, stenosis flow reserve provides the best arteriographic definition of stenosis severity, suitable as a gold standard for comparison with noninvasive imaging. Using stenosis flow reserve as the gold standard, PET has a diagnostic accuracy of 95%–98%, even in asymptomatic patients (*1,32,35*).

The quantitative severity of coronary artery stenosis correlates with severity of corresponding PET perfusion defect on rest-dipyridamole studies. Severity of PET perfusion defects read by two readers blinded to clinical or arteriographic data and graded visually on a severity scale from 0 (normal) to 5 (most severe) correlates well with arteriographic severity of disease. This relation between defect severity by PET and stenosis flow reserve by quantitative coronary arteriography is shown in Figure 7.

Localization of the artery(s) involved is highly specific for PET, as shown in Table 2. Since spatial localization is so good, lesions in series can routinely be identified by more severe defects distally, e.g., a septal perfusion defect and mild anterior defect as illustrated previously in Figures 3 and 5.

EXERCISE THALLIUM IMAGING AND DIPYRIDAMOLE PET

As shown in Table 1, the average sensitivity and specificity of thallium exercise testing in the last 3,119 cases published since 1983 are 84% and 53%, respectively, weighted for number of cases in each study. Sensitivity and specificity of exercise thallium imaging was 80%–90%

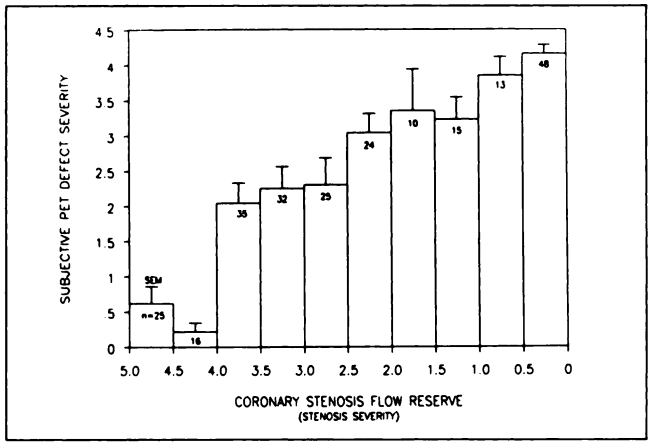

FIGURE 7. Visually scored severity of PET defects from 0 (normal) to 5 (severe defect) is related to stenosis flow reserve by automated quantitative coronary arteriography. Reproduced with permission from reference (*1*) as adapted from reference (*35*).

in symptomatic patients in literature prior to 1983 (*103–105*). Studies since 1983 report sensitivity of 70%–85% and specificity of 45%–60% in both symptomatic (*106–111*) and asymptomatic subjects (*112,113*) or those with atypical presentations (*114*), as summarized in Table 1. An average specificity of 53% means that there are 47% false-positive thallium exercise tests in patients whose coronary arteriograms show no significant coronary artery stenosis. These arteriograms are unnecessary if a more accurate noninvasive test is used initially. European experience with thallium SPECT confirms this low specificity (*115*).

One explanation proposed for low specificity in recent reports is "referral bias"; i.e., patients with negative thallium stress tests no longer undergo cardiac catheterization (*107,109*). The catheterized population in such a study would be biased by this exclusion of normals, thereby skewing the population toward higher prevalence of disease. According to Bayes' Theorem, as the population is skewed toward greater prevalence of disease, the post-test probability of having no disease with a normal test and the observed apparent test specificity decrease in that population (*116,117*).

However, we have demonstrated that the currently reported low specificity of 50%–60% is unlikely due to referral bias (*116–118*). Accounting for referral bias by a sophisticated model, Diamond (*118*) estimated an average "corrected" sensitivity of thallium exercise testing of 67.5% and average "corrected" specificity of 75% (Table 1). His conclusion agreed with our estimates of 65% sensitivity and 65% specificity accounting for changing patterns of interpretation since the early 1980s but without correction for referral bias (*116,117*). Although referral bias is a valid concept, it cannot be invoked to explain away the limited sensitivity and specificity of thallium exercise testing as currently used. Diamond also concluded that the use of

TABLE 2
Artery Localization

Stenosed Artery by Arter.	PET No.	PET Defect: Ant.	Sep.	Lat.	Inf. Post	None
None	32					*
	34					*
	35					*
	43					*
	44					*
	46					*
	47					*
	48					*
	63					*
	67					*
	68					*
	82					*
	83					*
	90					*
	91					*
	121					*
	160					*
	164					*
	167					*
	192					*
	242					*
	274					*
	310					*
	341					*
	343					*
	357					*
	361					*
	370					*
	434					*
	447			■	■	
	471					*
	475					*
	490					*
	511					*
	522					*
	525	■				
	539					*
LAD and/or Diagonal	49	○				
	54	○				
	71	○				

Stenosed Artery by Arter.	PET No.	PET Defect: Ant.	Sep.	Lat.	Inf. Post	None
LAD and/or Diagonal Con't.	136	○				
	146	○				
	153	●				
	181	●				
	217	○				
	236	●				
	238	○				
	507	○				
	78	○	○			
	333	○	○			
	417	○	○			
	246	●		●		
	384	○		○		
	137	○			○	
	142	●			●	
	241	○	○	○		
	503	○		○	○	
	243		○	○	○	
	70	●	●	●	●	
	61					●
	73					●
	80					□
	102					●
	129					●
	149					●
	152					●
	197					●
	229					●
	302					□
	307					●
	350					●
	351					●
	415					●
	424					●
Left Circumflex (LCX)	77			○		
	79	●				
	232				○	
	316				○	
	38			○	○	
	154			●	●	

Stenosed Artery by Arter.	PET No.	PET Defect: Ant.	Sep.	Lat.	Inf. Post	None
Left Circumflex (LCX) Con't.	162			○	○	
	195			●	●	
	206				○	
	233			○	○	
	273			○	○	
	315			○	○	
	322			○	○	
	330			●	●	
	481			○	○	
	56					□
RCA	75				○	
	84	○‡				
	135				○	
	385				○	
	396	○†				
	425				○	
	469				○	
	473				○	
	491				○	
	556	●‡				
	52	○‡			○	
	134	○		○		
	240			○	○	
	278			●	●	
	369	●		●		
	400		○		○	
	474	○‡			○	
	483		○		○	
	557	○‡			○	
	183					●
	376					□
	495					●
LAD and LCX	95	○				
	459			○		
	59	○	○			
	237	○		○		
	334	○		○		
	388	●			●	
	524	○		○		
	552	○			○	

Stenosed Artery by Arter.	PET No.	PET Defect: Ant.	Sep.	Lat.	Inf. Post	None
LAD and LCX Con't.	579	○			○	
	257	○		○	○	
	332	○	○	○		
	540	○	○	○		
	542	○		○	○	
	62					●
	196					□
	403					□
	460					□
LAD and RCA	64	●				
	532	○			○	
	207		○		○	
	211	○			○	
	221			○	○	
	394	○		○		
	81	○	○		○	
	117	○	○		○	
	251	○	○	○	○	
	309	○		○	○	
	180	○	○	○	○	
	297	○	○	○	○	
	560	○	○	○	○	
LCX and RCA	101				○	
	220				○	
	346				●	
	353			○		
	72	○			○	
	191		○		○	
	340			○	○	
	367		○		○	
	429			○	○	
	445			○	○	
	489			●	●	
	591			○	○	
	143					●
	381					●

Stenosed Artery by Arter.	PET No.	PET Defect: Ant.	Sep.	Lat.	Inf. Post	None
LM and LAD	163	○		○	○	
	502					●
LM and LCX	382				●	
LM and RCA	60	○	○	○	○	
LM and RCA and CX	500			○	○	
	325				○	
LAD and CX and RCA	98	○	○			
	314	○	○			
	342	○			○	
	345	○		○		
	554		○		○	
	139	○	○	○		
	252	○		○	○	
	380	○		○	○	
	413	○	○	○	○	
	438	○	○	○	○	
	545	○		○	○	
	561	○	○	○	○	
Revascularized after MI MI Location Anterior	306	*				
	479	*				
	395	*		*		
	277	*	*	*		
	281					*+
	282					*+
Antero-Lateral	288	*	*	*		
	317	*		*		
Lateral	435	*		*	*	
Infero-Posterior	222				*	
	397				*	
	194		*		*	
	279		*		*	
	323		*		*	
	173		*	*	*	
	464			*	*	
	480	*	*			
	421					*+
	484					*+

‡ Apical only
† S/P Ant. MI revascularized
+ Acute Reperfusions

○ Patients with significant CAD (CFR < 3) by QCA.
● Patients with mild CAD (CFR 3-4) by QCA.
□ False negatives: patients with significant CAD and normal PET.

■ False positives: patients with no significant CAD (CFR ≥ 4) by QCA and abnormal PET.
* Patients with no significant stenoses (CFR ≥ 4) by QCA

low risk groups to establish "normalcy" standards without comparison to coronary arteriography is not correct.

Table 1 compares currently reported sensitivity and specificity of thallium exercise testing, 84% and 53% respectively, with dipyridamole PET, 96% and 96% respectively (*1,32,35–37,119*). In a study population with a high prevalence (94%) of severe advanced CAD as reported by Tamaki (*120*), the differences between PET and thallium SPECT are not apparent (*120*) because the disease is severe enough to cause such high contrast between normal and abnormal areas of images that it is detectable even by limited technology. In addition, at a disease prevalence of 94%, the poor specificity of any modality is not manifest because there are too few normals (3 normals in the study) or those with less severe disease in the study population. Finally, the Tamaki study used treadmill exercise, which does not increase coronary flow as much as dipyridamole used in other PET reports. The advantages of advanced PET technology are best observed for intermediate disease prevalence (<60% of the study population) and/or moderate-to-less severe CAD in which the question of medical or mechanical intervention is unclear and thallium-stress testing is least accurate.

In two other studies directly comparing PET and SPECT (*121–123*), the diagnostic accuracy of PET was significantly higher than SPECT despite inadequate counts (6–7 million counts per whole-heart data set) in one study (*123*) and inappropriate PET software in the other (*121,122*), as previously analyzed in detail (*1*). Using a faster scanner collecting adequate counts (30–50 million counts per whole-heart data set) and optimized PET software, others have reported much better sensitivity and specificity of 95% or higher (*32,35–37,119*). A direct comparison of PET and SPECT has been reported using appropriate software, an appropriate study population, and adequate counts in a subset of 46 patients (*35*). Of those patients with moderately severe disease with stenosis flow reserve of < 3 by automated quantitative coronary arteriography, blinded readers identified 95% by PET compared with 58% by thallium exercise testing. Of those with milder disease with stenosis flow reserve between 3 and 4, PET detected 52% whereas thallium exercise testing detected none. Thus, a total of three studies with direct comparison of PET and SPECT showed PET to have better diagnostic accuracy than SPECT (*35,121–123*).

Technical Differences Between PET and SPECT

Although thallium treadmill testing and dipyridamole PET are both used for "stress" perfusion imaging, there are major differences between these two procedures. SPECT lacks attenuation correction, has depth-dependent changes in resolution, and limited sampling frequency. Of these, the lack of attenuation correction is the major problem because attenuation of activity from the inferior wall of the heart and septum (in men) and anterior wall (in women) is dependent on highly variable body habitus and orientation of the heart in the chest. Therefore, assumed constant or "standardized" distribution of attenuation corrections is not useful but must be measured.

Figure 8 illustrates the importance of attenuation correction (*1,31*). A rest perfusion image with N-13 ammonia was reconstructed by standard PET techniques with attenuation correction, upper panel labeled S1. The lower of each image pair, labeled S2, was reconstructed from the same data without the attenuation correction. Figure 8A shows short axis views and 8B shows polar map displays. The S2 images are therefore ideal SPECT scans collected with 360° of spatial sampling and high radionuclide energy (511 keV), thereby minimizing attenuation losses compared to much lower energy thallium or technetium. The SPECT image from the same data without attenuation correction shows severe inferior and septal defects typical of false-positive defects associated with tissue attenuation on thallium or technetium SPECT scans. Therefore, the high number of false-positive SPECT scans, or low speci-

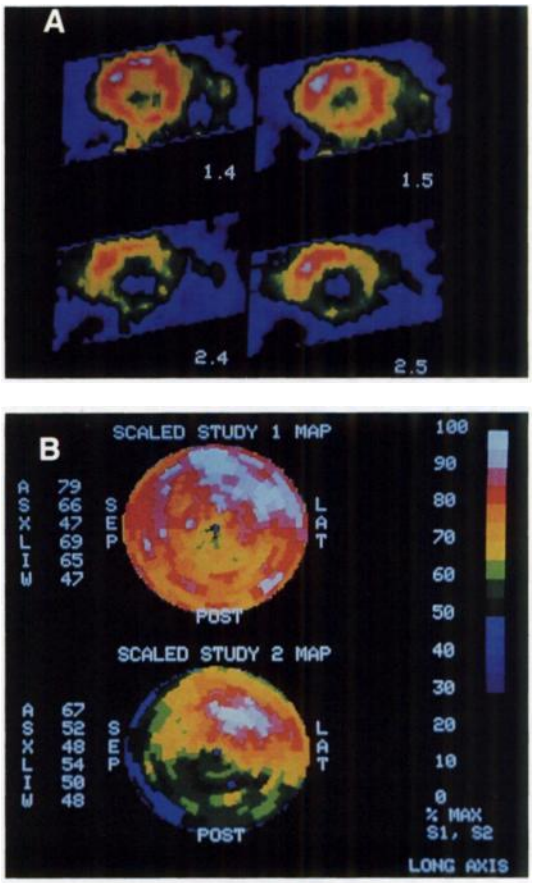

FIGURE 8. Resting myocardial perfusion scan using ^{13}N-ammonia with standard PET reconstruction using attenuation correction (S1) and without attenuation correction (S2). Lack of attenuation correction causes a severe inferior defect that is artifactual due to tissue attenuation in short-axis views (A,B). Reproduced with permission from reference (*1*).

ficity, can be explained by lack of attenuation correction as illustrated in this example, which cannot be distinguished from a real perfusion defect.

The three-headed SPECT scanner does not solve this problem but may make it worse. Artifactual inferior or septal defects appear to be as common or more common with the three-headed SPECT system compared with standard SPECT. The reason is that the better sampling of the three-headed SPECT system shows more clearly the attenuation of photons from posterior wall and septum. As imaging technology improves from planar to rotational SPECT to three-headed SPECT to complete ring SPECT, attenuation correction becomes increasingly important. Even with PET, as resolution and sampling frequency improve in more advanced PET scanners, attenuation correction becomes more critical and more difficult to do accurately.

The claim is often made that attentional losses with SPECT are less than with PET because single photons have a shorter path to the detector than the total path of the paired photons of positron decay. This claim is not compatible with basic fundamental physics of tomographic imaging. If a single photon arises from the anterior myocardium, it travels a shorter path and has less attenuation than paired photons from the same point detected in coincidence, since the path of paired photons includes the posterior attenuation. For the total path of all single-emission photons from inferior and septal areas of myocardium, attenuation is the same for coincidence- and single-photon counting, which causes inferior and septal defects unless corrected by transmission data. Attenuation from inferior and septal myocardium is unpredictable depending on cardiac size and orientation in the chest. Although overall attenuation by the entire heart is the same for single and paired photons for adequate circumferential sampling, the difference is that attenuation is measured and corrected by PET but not with SPECT.

The higher energy technetium compounds for SPECT have been thought to decrease the problem of artifactual inferior and septal defects due to attenuation. However, in our experience, higher energy emission does not reduce this problem. The images in Figure 8 were obtained with 511-keV emission of a positron radionuclide. Without attenuation correction, there is an artifactual severe inferior and septal defect. There are other causes for false-positive SPECT scans (*124*) as well as other technical details of PET relating clinical diagnostic accuracy to scanner performance (*1*).

Exercise stress does not increase coronary blood flow as much as i.v. dipyridamole or adenosine. Using PET to measure absolute coronary flow and coronary flow reserve, Schwaiger observed the normal increase in coronary flow with treadmill exercise to be 2.5 times baseline, compared with 4.1 times baseline for i.v. dipyridamole (Schwaiger M, personal communication, 1990). The stronger stimulus for increasing coronary flow (dipyridamole) increases its sensitivity and specificity for detecting and quantifying severity of coronary artery stenosis (*32–35,40,45–50*).

CARDIAC PET IN CLINICAL PRACTICE

Clinical cardiac PET utilizing the ^{82}Rb generator (*23, 24,35,36,58,63*) is practical in cardiologic practice (*119, 125,126*). Since the first private practice PET study in March, 1988 in Atlanta (*119*), over 4,000 patients have been studied in private practice sites. However, some qualifications are important to mention. Based on our experience in over 1,000 university-based clinical studies and the private practice studies, it is necessary to simultaneously utilize all tomographic views available for interpretation—acquisition, short-axis, long-axis, and polar map views. Short-axis views alone commonly fail to show abnormalities seen on long-axis views. For "balanced" three-vessel CAD, the polar map displays showing relative and absolute flow reserve of the whole heart demonstrate abnormalities more accurately than the tomographic views alone.

It is also our observation that PET data cannot be processed with software designed for SPECT imaging because the different reconstruction filters, rotational algorithms, etc. optimal for SPECT are unsatisfactory for PET images. Although the diagnostic accuracy of PET data processed by SPECT software is better than that by SPECT imaging (*121,122*), PET images processed with SPECT software are overly smoothed with data displaced into neighboring pixels (blurring) by multistep rotational schemes or excessive smoothing. Even with inappropriate software, specificity of PET for diagnosis of CAD was higher than for SPECT (*121,122*), but neither sensitivity nor specificity was as high as reported by others with appropriate software, i.e., Schelbert (*36*), Tamaki (*37*), Williams (*119*), Gould (*32*), and Demer (*35*). In our experience, suboptimal processing of PET data by SPECT software lowers diagnostic content in comparison with software specifically designed for PET reconstruction and display (*41*), which achieves a higher diagnostic accuracy (*32,35–37,119*).

Another reason for lower sensitivity (or specificity) is inadequate total counts in the whole-heart image set. Six to 7 million counts per whole-heart image set, as reported with a block camera design having high dead-time losses (*123*), seriously compromises diagnostic content for short-lived tracers like ^{82}Rb or ^{15}O-water. In comparison, for ^{82}Rb we acquire approximately 15–35 million counts per whole-heart data set and achieve a greater sensitivity and specificity. In count-poor studies, summing slices makes them look better but does not overcome the basic inaccuracy due to inadequate counts in the whole-heart data set. Therefore, high count rate capacity, good Z-axis sampling without interplane undersampling (*127–130*), and quantitative validated, clinical software (*41*) are important for achieving high sensitivity and specificity in clinical applications.

ECONOMICS OF PET USING ^{82}Rb AND BASIS FOR INSURANCE REIMBURSEMENT

Figure 9 (*132*) shows the comparative diagnostic costs of PET, SPECT, or arteriography as a function of CAD prevalence in the study population (*1,131–133*). For this figure, sensitivity and specificity for SPECT were 80% and 50% respectively and, for PET, 95% and 95% respectively, as shown in Table 1. Cost of SPECT was $1,000 per study, including professional fees, cost for PET using generator-produced ^{82}Rb was $1,500. Each positive noninvasive test by both technologies was assumed to incur arteriography costing $6,000. If the cost of coronary arteriography for false-positive tests is counted into the cost of identifying or ruling out disease, the overall expense of medical care utilizing thallium SPECT is higher than for PET due to costly definitive catheterization required for false-positive SPECT results.

Since PET also provides an approximate quantitative assessment of severity, it can potentially be used as a substitute for arteriography in many patients with mild to moderate disease amenable to medical therapy. If approximately 30%–40% of patients undergoing coronary arteriography who need a mechanical procedure (PTCA, bypass surgery) could be identified by PET, the need for many arteriograms could be prevented. This instance is shown by the lower line of Figure 9 where half of the arteriograms have been eliminated on the basis of PET results showing mild disease. On the other hand, individuals with asymptomatic severe disease identified by PET may need mechanical intervention to prevent myocardial infarction or sudden death. Therefore, the use of the ^{82}Rb generator instead of a cyclotron for cardiac PET reduces the cost of PET imaging to a reasonable range for routine clinical use as the basis for vigorous medical therapy or mechanical intervention.

If medical insurers are willing to pay for thallium, which has a published accuracy of only 50%–60% and leads to additional costs of unnecessary coronary arteriograms, then they should ensure payment for PET, which is more accurate and provides additional diagnostic certainty on severity/location of coronary artery stenosis, which is crucial for determining the need for PTCA or bypass surgery. PET diagnosis can eliminate the need for additional unnecessary arteriograms by determining that a disease is not severe enough and/or not critical in area or size, e.g., a small defect in the right coronary artery distribution, to require arteriography. Thus, PET provides independent hard data that can determine subsequent treatment of patients at cost savings to the insurer.

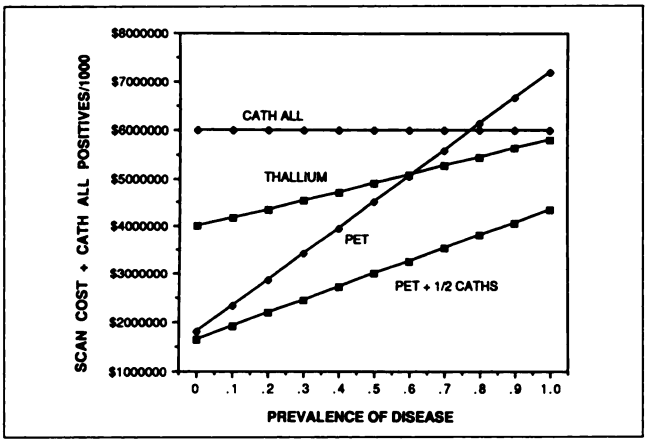

FIGURE 9. Comparative costs of ^{201}Tl SPECT and PET with generator-produced ^{82}Rb as a function of disease prevalence. Reproduced with permission from reference (*132*).

ADDITIONAL BENEFITS OF PET WITH ^{82}Rb: ASSESSING MYOCARDIAL INFARCTION, ISCHEMIA AND VIABILITY

Distinguishing necrotic from viable myocardium is important for treating patients with acute myocardial infarction, particularly following thrombolysis therapy when revascularization or balloon angioplasty may be indicated for remaining viable myocardium. The extent of myocardial infarction and/or viability depends on how it is measured. Thallium exercise perfusion imaging in the peri-infarction period is most commonly used for this purpose (*134–141*).

For example, Rozanski et al. (*135*) reported in 1981 that 35 out of 43 patients (81%) with stress defects that redistributed on ^{201}Tl exercise tolerance tests (ETT) improved left ventricular wall motion after bypass surgery. However, 19% with reversible stress defects did not improve. Although most patients with fixed defects on ^{201}Tl ETT did not show improved wall motion, 4 of 29 did improve despite fixed defects. In 1989, Tamaki et al. (*56, 139*) found that 8 of 23 myocardial segments (35%) with transient defects on ^{201}Tl ETT SPECT did not improve left ventricular function postoperatively; 14 of 33 patients with fixed defects (42%) did improve left ventricular function postoperatively (*56*).

In 1988, Cloninger et al. (*137*) reported that of 95 patients with first suspected or documented myocardial infarction and incomplete redistribution on ^{201}Tl ETT, 72 (76%) improved redistribution images and 24% did not improve after PTCA. Of 16 patients with prior or acute myocardial infarction and incomplete redistribution, 8 improved redistribution images after PTCA and 8 did not (*137*). These reports suggest that identifying myocardial viability and postoperative improvement in left ventiricular function by stress thallium imaging without reinjection has limited predictive accuracy for improvement after mechanical intervention and is therefore limited for assessing viability.

Of the many possible reasons for ^{201}Tl ETT failing to predict viability, two possible explanations stand out: either the imaging technology of ^{201}Tl is inadequate or the basic concept of identifying necrosis by a fixed defect on ^{201}Tl ETT is incorrect. With regard to the first alternative, exercise perfusion imaging of ^{13}N-ammonia by PET does

not improve prediction of postoperative improvement of left ventricular function (*56,139*). Fourteen of 48 segments with transient perfusion defects by ^{13}N-ammonia and PET (30%) had no improvement in left ventricular function postoperatively; 5 of 27 segments with fixed defects (19%) had improved left ventricular function despite fixed defects (*56*). Therefore, in the same study, the errors of exercise perfusion imaging for predicting viability and postoperative improvement in left ventricular function was 35%–42% for SPECT and 20%–30% by exercise perfusion PET imaging.

Therefore, the error of 20%–30% in predicting viability and postoperative improvement in left ventricular function based on transient stress perfusion defects may be due in part to a problem with the basic concept of exercise perfusion imaging as a means of assessing viability.

Figure 10 (*1*) shows schematically a defect in both stress (left panel) and redistribution (right panel). Due to washout of thallium from the normal area on the 4-hr redistribution scan, the relative severity of the defect appears to decrease as if redistribution into the defect had occurred, suggesting viability. However, the apparent partial redistribution may be due to washout of radionuclide from normal area with decreasing severity, i.e., a "reversible" defect. Similarly, a rest PET perfusion scan will have a less severe defect than the exercise PET perfusion scan due to greater uptake of radionuclide by normal myocardium. Therefore, no information is provided about viability in the area of the resting defect since apparent lessening of defect severity may be due to washout of activity from the normal area or lower resting flow compared with stress flow in normal area.

Figure 11 (*1*) illustrates that a partly reversible exercise perfusion defect identifies the area of limited flow reserve around a central injured area of myocardium (left panel). It does not provide data on how much viable myocardium is left in the area of the defect with potentially partial damage. Exercise or dipyridamole stress perfusion imaging therefore provides a measure of the zone at risk having low flow reserve (right panel) but not of viability within the area of a fixed defect.

Positron emission tomography has been developed for identifying ischemic, viable, or necrotic/fibrotic myocardium by imaging metabolic analogs, especially [^{18}F]FDG, and/or cell membrane integrity by the potassium analog ^{82}Rb, as outlined below.

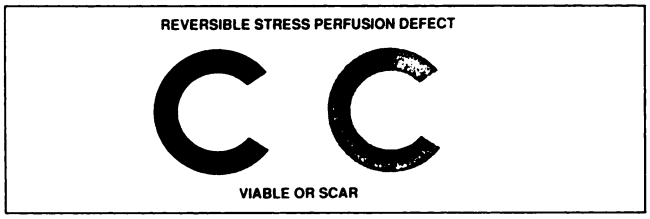

FIGURE 10. Schematic representation of thallium washout from normal areas of an exercise image (left panel), resulting in relative redistribution on the 4-hr delayed imaged (right panel), which is consistent with either scar or viable myocardium. Reproduced with permission from reference (*1*).

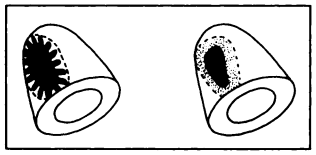

FIGURE 11. Schematic of an enlarging or worsening defect with stress compared to the central resting defect of a rest or redistribution thallium image. This partially reversible defect indicates the area of low flow reserve around a central resting defect but does not provide information on the viability (or necrosis) of myocardium within the resting defect. Reproduced with permission from reference (*1*).

PROTOCOL FOR MYOCARDIAL VIABILITY AND INFARCT SIZE WITH ^{82}Rb

The leak of potassium from myocardial cells is an immediate early marker of impaired cell membrane function and necrosis that has been well documented by a substantial literature (*1,142,143*). Therefore, a quantitative imaging method utilizing a potassium analog reflecting cell membrane function might be useful for assessing viability and infarct size.

Rubidium is a potassium analog with a variety of medically useful radioactive forms including ^{81}Rb, ^{82}Rb, ^{84}Rb, and ^{86}Rb. Myocardial cell membrane transport, trapping, and flow-extraction characteristics of potassium and rubidium parallel each other.

The clinical protocol based on rubidium kinetics utilizes the same resting perfusion protocol described previously with the exception that the image data is acquired in list mode. As illustrated in Figure 12 (*144*), the resting PET data collected in list mode is divided into an early phase

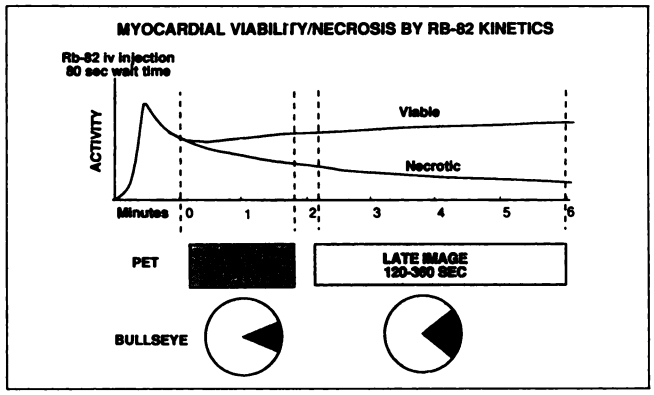

FIGURE 12. Schematic of the clinical protocol utilizing the kinetic changes of ^{82}Rb after intravenous injection for assessing myocardial viability. Reproduced with permission from reference (*144*).

image (first 15–110 secs) and a late phase image (120–360 secs). A new defect or worsening defect on the late image compared with the early image indicates washout or failure to trap rubidium and therefore necrosis. Residual myocardial trapping of rubidium on the late image within a defect reflecting partial or limited washout indicates some residual viable myocardium.

Infarcted myocardium fails to retain rubidium, which washes out from cells after initial uptake. A mix of infarcted and viable tissue in the field of view results in an intermediate level of washout proportional to the percent of viable or infarcted tissue. The activity in the late (S2) rubidium image relative to the early (S1) image therefore reflects the extent of washout and proportion of viable or necrotic myocardium.

Figure 13 (*41*) shows early (S1) and late (S2) images after a single i.v. injection of generator-produced ^{82}Rb in a patient with an evolving acute anterior myocardial infarction in horizontal and vertical long axis views. The early images are shown uppermost in each pair of image rows (study 1). The late images are in the lower row of each pair of image rows (study 2). The number after the decimal is the image plane for both studies 1 and 2. In the color coding, white indicates the highest activity, red next highest, yellow intermediate, and green and blue the lowest relative activity.

Figure 13A shows horizontal (left) and vertical (right) long axis views of the heart. The horizontal long axis views are oriented as if looking down from above. The vertical long axis tomographs are oriented as if looking at the left side of the body cut head to toe. Anterior myocardium is at the top, inferior at the bottom, apex at the left, and AV ring on the right.

Tomographic data is summarized in a polar display as if looking at the patient from the outside toward the left ventricular apex located in the center of the bull's-eye with the outer rim of the bull's-eye corresponding to the AV ring. Polar displays on the left (lower half of figure) show the relative activity on a scale of 0%–100% with the early study being the upper (S1) and the late study being the lower (S2) of the polar maps on the left side of the panel. The lower right polar display, labeled relative S2/S1 ratio, shows the relative change in normalized activity of the late image divided by the relative distribution of normalized activity of the early image (relative instead of absolute values), on a scale of 0 to 2. It therefore quantifies the relative change in activity from early to late images (*144*). The upper right polar map, labeled absolute S2/S1 ratio, is used for comparing rest-stress images and has no meaning or use for comparing early-late images.

The patient in this figure is a 51-yr-old woman with acute anterior myocardial infarction 2 days previously. The early rubidium image (S1) shows normal perfusion to the anterior wall indicating a reperfused LAD that washes out to leave a severe defect at the apex indicating necrosis. The anterior wall retained rubidium indicating a substantial amount of viable myocardium remaining. As shown in Figure 13B, the late rubidium image (S1, upper row) matched the FDG image (S2, lower row) thereby confirming that substantial viable myocardium remained. Consequently, arteriography was carried out, which confirmed a reperfused LAD stenosis followed by successful PTCA. Follow-up PET showed a normal anterior wall and only a residual small apical scar.

Figure 14 (*144*) correlates infarct size based on rubidium washout compared with FDG images, both with automated infarct sizing, in the first 36 patients studied with both ^{82}Rb and FDG after glucose loading. The patients with very large infarct areas had previous infarctions and severe ischemic cardiomyopathy, and were being considered for cardiac transplantation. For these very large in-

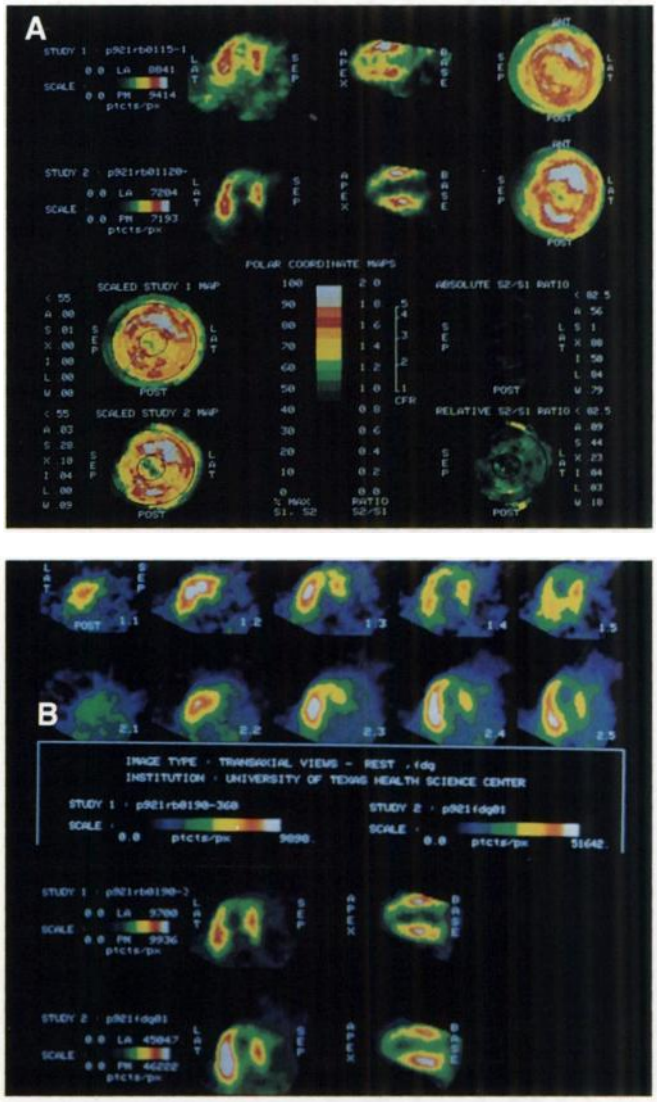

FIGURE 13. PET images early (S1) and late (S2) after a single intravenous injection of ^{82}Rb at rest in long-axis views and polar maps (A). (B) The late rubidium image (S1) is identical to the FDG image (S2). See text for details. Reproduced with permission from reference (*41*).

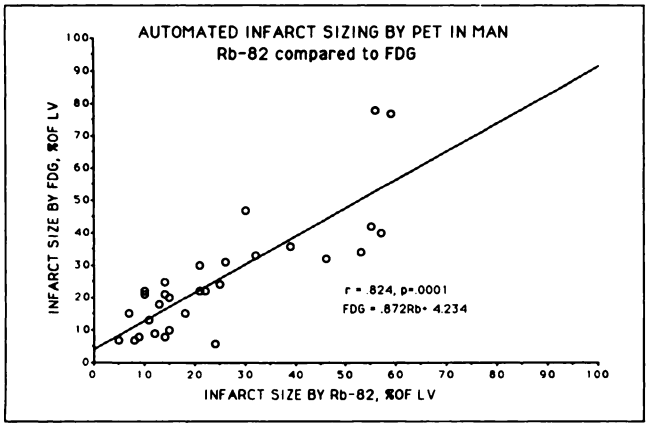

FIGURE 14. Infarct size based on rubidium images compared to infarct size by FDG images, both using automated computerized infarct sizing methods. Reproduced with permission from reference (*144*).

farct areas, the relation between infarct size by rubidium and FDG is less good, primarily due to probable overestimates by the FDG method since some of the largest infarct sizes by FDG would appear to be incompatible with survival.

Nine out of 43 patients with acute evolving myocardial infarction studied with FDG after glucose loading (21%) had no myocardial uptake anywhere in the heart or large areas of normal myocardium that did not take up glucose after glucose loading despite normal contraction and perfusion. Eight of these nine patients were diabetic (*144*).

Our results demonstrate that the size of infarcted myocardium defined by abnormal rubidium kinetics is comparable to the size of infarcted myocardium defined by lack of FDG uptake on PET images using appropriate glucose loaded protocols. They also indicate that in myocardial necrosis the loss of cell membrane integrity as reflected by abnormal kinetics of the potassium analog ^{82}Rb parallels loss of intracellular intermediary glucose metabolism as reflected by lack of FDG uptake. Our observations extend the well-described behavior of potassium as a marker of myocardial necrosis into clinical applications for infarct sizing and relate it to more recent measures of viability based on metabolic imaging. Thus, myocardial necrosis or viability may be identified by measures of either glucose metabolism or cell membrane integrity.

FDG IMAGING IN COMPARISON WITH ^{82}Rb

Metabolic imaging for myocardial viability is often considered the best validated advantage of PET over perfusion imaging with thallium or positron perfusion tracers. However, this claim is based on only two clinical reports involving a total of 39 patients in the world's PET literature (*57,141*), Table 3. The accuracy of FDG imaging for predicting improvement of poorly contracting LV segments after bypass surgery was 78% (*141*) to 85% (*57*), as compared with 65% (*56*) to 81% (*135*) for thallium. For comparative purposes, Table 3 also lists the major clinical imaging trials of PET involving 470 patients reporting a 95% or greater sensitivity and specificity for the diagnosis of coronary artery disease. The numbers of studies and relative improvement in diagnostic power supports the use of PET for perfusion imaging as much as for identifying viability and reversible wall motion abnormalities.

The initial report on FDG in 17 patients indicates that 85% of hypokinetic segments taking up FDG improved function after bypass surgery (*57*). However, ejection fraction improved significantly only in those with three or more segments involved. Data was not provided on the percent of patients with three or more viable regions that

TABLE 3
Comparison of Clinical Imaging Trials for Patient Management of Viable Myocardium

Diagnostic Test	Accuracy		Patients	Reference
	Pos	*Neg*		
Predicting improved postop	85%	92%	17	Tillisch (57)
left ventricular wall motion	78%	78%	22	Tamaki (139, 141)
by FDG				
Predicting improved postop	81%	86%	25	Rozanski (135)
left ventricular wall motion	65%	58%	31	Tamaki (56)
by T1201	86%	78%	26	Iskandrian (136)
	Sn	*Sp*		
Diagnosis of coronary artery stenosis using ^{82}Rb	95%	100%	50	Gould (32)
	94%	95%	193	Demer (35)
with a fast PET scanner or	97%	100%	32	Schelbert (36)
$^{13}NH_3$	97%	100%	49	Yonekura (37)
	98%	93%	146	Williams (119)

would warrant bypass surgery or the percent of patients showing improved ejection fraction.

Since FDG imaging is currently used for assessing myocardial infarction and viability (*61*), it is important to emphasize the conditions under which it is applicable and those under which it is not reliable fo assessing ischemia viability and necrosis. After oral glucose loading in chronic CAD and acute myocardial infarction, myocardial areas with a rest perfusion defect and increased FDG uptake after glucose loading (flow-metabolism mismatch) are hypothesized to be viable and may demonstrate improved left ventricular function after revascularization (*57,61*). Areas with a perfusion defect and low FDG uptake after glucose loading (flow-metabolism match) identify necrotic or fibrotic myocardium showing no improvement after revascularization. After fasting and exercise stress in chronic CAD, FDG uptake identifies ischemic viable myocardium as a positive image with no uptake in normal or necrotic tissue (*44,61,65–67,71*).

However, there are several circumstances in which myocardial FDG uptake is not consistent or predictable and therefore fails to differentiate necrotic from viable tissue (*1,144–147*). Normally perfused and contracting myocardium of some diabetic patients may not take up FDG either with or without glucose loading, even after their usual dose of insulin and/or oral hypoglycemic agents. This failure of FDG uptake in diabetics after glucose loading may erroneously suggest necrosis when the myocardium is normal. In such instances, perfusion imaging or measures of cell membrane integrity discussed subsequently are the major guides to viability or necrosis for clinical decisions on intervention.

In the fasting state at rest in normal and diabetic subjects, FDG uptake either with or without evolving myocardial infarction is so variable as to be uninterpretable. Additionally, after fasting and at rest in the setting of acute evolving myocardial infarction, intense FDG uptake may occur in areas of myocardium that are necrotic-documented by lack of FDG uptake after glucose loading, left ventricular akinesis, and arteriographic involvement of the corresponding coronary artery (*144–146*). A similar observation has been made in experimental animals using cardiac autoradiography (*147*). For these patients, necrotic tissue erroneously appears viable due to intense FDG uptake. In our early experience before recognizing these problems, two such patients had bypass surgery on the basis of intense FDG uptake in the occluded artery distribution but demonstrated no recovery of function and remained in chronic heart failure postoperatively despite open bypass grafts (*144–146*). Therefore, we now do not carry out FDG imaging in the fasting, resting state in acute evolving myocardial infarction.

Pierard et al. (*146*) showed that a large proportion of patients with myocardial infarction and myocardial areas of intense FDG uptake did not improve LV function in these areas after bypass surgery; at 9-mo follow-up, FDG scans showed fibrosis in these areas suggesting that FDG uptake in the setting of acute myocardial infarction does not indicate viability.

The mechanism for FDG uptake in recently infarcted myocardium is unclear. In experimental chronic cerebral infarction, elevated FDG uptake is observed in infarcted tissue in association with white blood cell phagocytosis of cellular debris (*148*). In areas with highly active phagocytosis, the intensity of FDG uptake in chronic cerebral infarction may be higher than FDG uptake of normal brain. FDG uptake by white blood cells in myocardial infarction in acute short term experiments (6 hr) is insufficient (*149*) to explain these observations. However, longer term experiments on white blood cell uptake of FDG in evolving myocardial infarction comparable to those observed for cerebral infarction or comparable to our observations in man have not been carried out. Consequently, observed FDG uptake in evolving myocardial infarction after fasting may be associated with phagocytic activity of white blood cells as found in cerebral infarction.

Myocardial uptake of FDG is also highly dependent on substrate availability (*150*) and catechol levels (*151*), thereby reflecting many conditions aside from viability. When myocardial uptake of FDG is unpredictable or taken up in myocardium by unclear mechanisms perhaps unrelated to viability, the application of quantitative models for deriving absolute glucose utilization in g/mg/min is inappropriate. Even under usual circumstances, absolute measurements of myocardial flow or glucose consumption in the myocardium or brain do not appear necessary for patient studies since most clinical reports showing the real benefits of PET imaging use end points of relative FDG uptake or relative uptake of a perfusion tracer.

Finally, in contrast to chronically reduced resting flow to viable myocardium, reperfused myocardium during acute myocardial infarction makes interpretation of a perfusion-metabolism mismatch on FDG images quite complex. A defect on a perfusion image after reperfusion with a patent artery suggests a no-reflow phenomenon associated with necrosis and an FDG defect. Alternatively, perfusion may be normal or near normal, either with or without an FDG defect. In this case, a reverse mismatch may occur with no perfusion defect associated with an FDG defect, the significance of which has not been documented.

With reperfusion in acute myocardial infarction, the zone of myocardium at risk is not readily defined by a resting perfusion defect, which, in chronic stable CAD, is the basis for the perfusion-metabolism mismatch to define viable myocardium. Since most of our patients had received thrombolysis therapy in this study, we avoided these problems by using relative FDG uptake compared with normal myocardium (after glucose loading) without reference to a metabolism/perfusion ratio, which has not been demonstrated as diagnostically useful in the setting of acute myocardial infarction and/or reperfusion.

STRESS PERFUSION IMAGING FOR ASSESSING MYOCARDIAL VIABILITY

For thallium stress testing, stress perfusion defects not present at rest or redistribution indicate areas of limited coronary flow reserve that are measures of zones at risk, not viability per se. For severe stenoses that reduce resting flow, the defect severity on stress perfusion images may be more intense and/or larger than at rest simply because adjacent areas with normal flow reserve have greater perfusion tracer activity associated with higher stress flow unrelated to viability in the area of the defect. Thus, reversible stress defects reflect flow capacity of normal myocardium around a resting defect but do not provide information on viability of myocardium within a resting perfusion defect.

With reperfusion, the definition of viability becomes more complex since the zone at risk characteristically contains a mix of viable and necrotic tissue with a patent artery and adequate flow. In this case, stress-induced enlargement of a perfusion defect may indicate additional zones at risk with low coronary flow reserve around the damaged area or limited flow capacity in the central damaged region due to edema or obliteration of vascular channels. However, it does not provide information on whether there is viable myocardium in the more central reperfused area of injury. Similarly, the newer technetium imaging agents do not provide measures of viability nor reflect cell membrane integrity.

Although the concept of a perfusion-metabolism mismatch is important and often predicts viable myocardium in resting defects, its general clinical applicability may be somewhat limited due to the difficulty of defining a perfusion zone at risk under resting conditions and/or after reperfusion. Consequently, we utilize FDG uptake and/or rubidium washout at rest not only with reference to resting perfusion but also compared with dipyridamole defects, in order to completely evaluate the proportion of viable or necrotic myocardium mixed together in the resting defect as well as the zone at risk defined by limited flow reserve.

From a study of rest-exercise PET using ^{13}N-ammonia, 34 of 48 segments with transient perfusion defects (71%) improved after bypass surgery (*56*). Of myocardial segments with transient reversible perfusion defects on thallium exercise imaging, 65% (15/23) (*56*) to 81% (35/43) (*135*) respectively improved after bypass surgery (*56,135*). Therefore, based on published literature, prediction of postoperative recovery in 78% (*141*) to 85% (*57*) of left ventricular segments taking up FDG is not much better than the improved postoperative function in 65% (*56*) to 81% (*135*) of left ventricular segments with reversible stress defects by PET perfusion or thallium perfusion imaging. Furthermore, studies of left ventricular segments do not reflect the proportion of patients with large enough viable areas to warrant interventions. Finally, identifying viable myocardium by the thallium reinjection technique has been shown to be comparable to FDG PET imaging (*152,153*).

COMBINED ASSESSMENT OF CORONARY FLOW RESERVE, MYOCARDIAL INFARCT SIZE, VIABILITY, AND ZONE AT RISK

As a measurement conceptually separate from infarct size and viability, we define the area of reduced flow reserve or zone at risk by dipyridamole perfusion imaging (*1,32,34,35*) rather than rest perfusion imaging. Therefore, we conceptually use the term "viability" of myocardium in reference to a nontransmural, mixed, or incomplete infarction as distinct and different from what is loosely termed in the literature as "viability" of areas with normal resting perfusion within a zone of reduced flow reserve or stress perfusion defect due to a stenotic artery. Imaging analogs of metabolism (FDG) or membrane function (^{82}Rb) identifies viability and necrosis in a mixed or incomplete infarction either with or without a resting perfusion defect with or without reperfusion. Dipyridamole or exercise stress perfusion imaging identifies zones of adequate resting flow but low flow reserve at risk of potential further necrosis. Thus, in the literature, viability is loosely defined depending on how it is measured.

Complete analysis of myocardial infarction requires assessing viability of myocardium in the central infarcted or partially infarcted myocardium at rest as well as the larger zones at risk around that region or in other parts of the heart with reduced flow reserve signifying proximal stenoses. Thus, complete clinical evaluation for a major intervention like bypass surgery or PTCA requires imaging coronary flow reserve and cell membrane integrity by the potassium analog ^{82}Rb or cell metabolism by the glucose analog FDG, and perfusion with ^{13}N-ammonia.

PRACTICAL CONSIDERATIONS FOR CLINICAL PET WITH ^{82}Rb

Although FDG is used for assessing myocardial viability, it requires a cyclotron and takes approximately 2 hr for the perfusion-metabolism study including the sequence of imaging ^{13}N-ammonia for perfusion, the time for FDG uptake, and FDG imaging for metabolic activity. This 2-hr period for one viability study limits the patient volume to approximately four per day, which may be below the minimum volume for "economic breakeven" depending on the clinical charge. Assessing myocardial viability with generator-produced ^{82}Rb at rest (without dipyridamole imaging) requires only 35 min to complete and therefore may be more practical from a clinical point of view.

For clinical applications, ^{82}Rb is well suited for assessing both viability/infarct size at rest and the zone at risk by dipyridamole perfusion imaging in a brief (1 hr) single study. The use of dipyridamole in the peri-infarction period is safe and useful for risk stratification (*1*). A rubidium washout study for infarct size is carried out as

part of a rest-dipyridamole sequence by collecting the rest data in list mode. Dipyridamole perfusion images using rubidium are then obtained. For the rest-dipyridamole comparison to define the zone at risk, all the list mode data are reconstructed into a single rest image and compared to the dipyridamole image. For the resting rubidium washout analysis to determine infarct size-viability, the rest data are divided into early and late rubidium images. Acquiring the entire data set for infarct size-viability and rest-dipyridamole images with ^{82}Rb requires 1 hr in our laboratory. The same sequence of viability and stress images with ^{13}N-ammonia and FDG requires 4–5 hrs due to longer data collection times for both these tracers, longer time for decay of ^{13}N-ammonia for rest-stress studies in sequence, and longer uptake period of FDG.

Thus, using rubidium kinetics to evaluate myocardial viability may have several advantages. First, it does not require the expense of a cyclotron. Second, the entire rest rubidium study takes significantly less time than for ^{13}N ammonia and FDG, thereby allowing higher patient volumes at reasonable cost. By combining washout measurements with dipyridamole stress using rubidium, complete information on viability of injured myocardium and stenosis severity of other myocardium at risk are obtained. Finally, it avoids the problems of inadequate FDG uptake in some diabetics and variable patient response to fasting or glucose loading.

REVIEW OF THE AMERICAN COLLEGE OF CARDIOLOGY (ACC) POSITION PAPER

The ACC report makes a number of factually incorrect statements as follows:

1. *Statement.* The major data on PET perfusion imaging are from only one large center. *Response.* As shown in Table 1, five papers from four centers have all reported comparable sensitivity and specificity of 95–98%, including Gould (*32*), Schelbert (*36*), Williams (*119*), Demer (*35*) and Yonekura (*37*). In comparison, seven papers from six centers published since 1983 report that the diagnostic specificity of thallium exercise testing in the last 3,119 cases is 53% and sensitivity is 84%, as shown in Table 1 (*106–114*). This limited specificity is further confirmed by reports from the most recognized SPECT experts in the United States (*111*) as well as in Europe (*115*). Two independent analyses (*116–118*) have ruled out referral bias to explain away this low specificity, including a report from the most recognized PET center (*118*). Uncathed "normalcy" rates are not appropriate substitutes for observed specificity (*116–118*). Low specificity is primarily due to lack of attenuation correction (*31*) and a number of other well-defined factors (*124*) that are not accurately corrected.

2. *Statement.* The best documented application of PET is for myocardial viability. *Response.* Table 3 shows that the validation of FDG by PET showing improved LV function is based on only 39 patients in the world's literature. Furthermore, other university centers have demonstrated major problems with using FDG for viability (*144–147,150,151*). These limitations include 20%–25% of studies being uninterpretable (*144,145*), intense uptake of FDG in necrotic myocardium (*144–147*) as evidenced by failure to improve left ventricular function after successful bypass surgery (*146*), and dependence of FDG uptake on substrate availability (*150*) and catechol levels (*151*). In comparison, Table 3 shows that there are more clinical cases from more centers validating high sensitivity and specificity for perfusion imaging than FDG for assessing myocardial viability. Finally, Bonow (*152,153*) has demonstrated that PET of FDG has no advantage over reinjection of thallium-201 for assessing viability.

3. *Statement.* Only one study reports a direct comparison between PET and SPECT, showing them to be equivalent. *Response.* In the study by Tamaki (*120*), the prevalence of disease was 94% with only three normals studied. This small number of normals does not permit determination of specificity, yet it was the main basis of the ACC report. Furthermore, this study population had advanced, severe, symptomatic clinical disease. For a population with such advanced disease, virtually any diagnostic modality is accurate, including a simple history. Finally, the Tamaki paper used treadmill exercise stress for patients on cardiac drugs, which blunt heart rate response. Other PET studies have used dipyridamole, which increases flow more than exercise does. However, even with this advanced disease population Tamaki concluded that PET was better than SPECT for regional localization of disease, a conclusion ignored by the ACC report. The study by Go (*121,122*) comparing PET with SPECT also utilized a population with advanced disease and processed the PET images with SPECT software displays that degraded the PET data. Despite these drawbacks the specificity of PET was better than SPECT. A direct comparison with an appropriate study population and appropriate hardware-software was made by Demer (*35*), whose study included a subset of 46 patients who had both PET and SPECT. Of patients with moderately severe CAD (coronary flow reserve of <3), PET identified 95%, whereas thallium stress testing identified 58%. Of patients with mild disease (flow reserve of 3–4), PET identified 52%, whereas thallium stress testing identified none. Thus, at each level of disease severity, the PET was considerably more accurate than SPECT. Therefore, 3 studies directly comparing the

two modalities (*35,121–123*) have shown PET to be superior to SPECT.

4. *Statement.* The specificity of PET was 74% in the single large study reported (*35*). *Response.* The ACC report misquotes the specificity, which was correctly reported in the peer-reviewed paper as 95%. The ACC committee members utilized an erroneous recalculation of specificity from peer-reviewed data based on their incorrect reclassification of patients. Their incorrect modification of this data was NOT peer reviewed. The committee review also ignored the subset of patients in that report with a direct comparison of PET and SPECT, as noted above. Despite this erroneous non-peer-reviewed miscalculation and misquote, several other centers have reported specificity of 95% including Schelbert (*36*), Tamaki (*37*), Williams (*119*), and Gould (*32*), comparable to the 95% reported by Demer (*35*) but misquoted in the ACC report.
5. *Statement.* The ACC report indicates a problem with availability of the ^{82}Rb generator. *Response.* Careful follow-up has indicated that not one member of the ACC committee contacted either the supplier (Squibb) or any rubidium clinical site to determine whether rubidium availability was a problem. The committee also overlooked Squibb publications and news releases establishing a public record of rubidium availability that has been confirmed by every clinical site.
6. *Statement.* The ACC report suggests that lack of approval of dipyridamole by FDA limits the use of ^{82}Rb for PET. However, the ACC report fails to indicate that no NDA for cyclotron-produced radiotracer has been approved by the FDA for commercial clinical use. However, rubidium now also has been approved. Intravenous dipyridamole for diagnostic imaging has been approved by the FDA for clinical use. It has been and is now used widely for both thallium and rubidium perfusion imaging under IND status in over 4,000 patients prior to FDA approval.

An initial report on clinical PET was approved by the ACC Imaging Committee in 1988 and circulated within ACC's administrative review committees. It was a careful, balanced review favorable to cardiac PET for both perfusion imaging and viability. However, this initial favorable report was subsequently revised by new and prior committee members, none of whom have clinical experience with ^{82}Rb and none of whom routinely carry out or have published data on routine clinical PET perfusion imaging for managing cardiac patients.

CONCLUSION

Cardiac PET using ^{82}Rb has proven accurate, nearly as definitive as the coronary arteriogram, and economical in multiple university and private practice sites for routine, high volume, cardiac diagnosis and management for the following indications:

1. Diagnosing and assessing severity and location of coronary artery stenosis in patients with angina pectoris, atypical chest pain, or risk factors for coronary artery disease, to determine the need for arteriography, medical, or mechanical intervention.
2. Identification of additional myocardial areas at risk and myocardial viability/necrosis in patients with evolving or old myocardial infarction, thereby establishing the need for arteriography, medical, or mechanical intervention.
3. Evaluation of collateral function which, if adequate under appropriate circumstances, may make mechanical intervention unnecessary.
4. A more accurate substitute for current standard exercise perfusion imaging done for whatever conditions are medically indicated.
5. Ruling out significant coronary artery disease with a high specificity in patients who would otherwise have an exercise stress test with poor specificity leading to unnecessary arteriography.

Traditionally in medicine, the patient and physician wait until angina pectoris, myocardial infarction, arrhythmia, heart failure, or sudden death leads to medical or mechanical intervention. However, symptoms are usually late manifestations of advanced disease in which reversal of coronary artery stenosis is difficult and mechanical procedures are often necessary. As a guide to therapy, angina pectoris usually indicates severe coronary artery stenosis, does not predict sudden death or acute myocardial infarction, and can be improved or eliminated by medical therapy without affecting progression of disease. By the time angina pectoris develops, the optimal opportunity for reversal therapy has passed. Consequently, diagnosing coronary artery stenosis and its severity at the mildest, earliest possible stage, particularly before symptoms, is important for instituting vigorous risk factor modification.

Although reactive treatment triggered by symptoms appropriately remains central to cardiovascular medicine, advanced diagnostic and therapeutic technology provide the opportunity for another major step in the evolution of cardiovascular medicine. PET has sufficient diagnostic power for a new therapeutic approach based on routine, economical noninvasive diagnosis and assessment of severity in symptomatic or asymptomatic individuals with intense dietary or medical treatment for reversal of CAD. Such therapy is not appropriate for the general population or for individuals without known coronary artery stenosis or a specific genetic susceptibility to it. This approach is therefore targeted, individually specific, preventive intervention. For severe silent disease identified by PET, coronary arteriography and mechanical intervention may be

indicated to prevent myocardial infarction or sudden death.

In contrast with the traditional approach based on symptoms, this new approach is based on functional and anatomic characterization of stenoses and myocardial viability with sufficient reliability in symptomatic or asymptomatic patients to justify medical or mechanical interventions having significant benefits and risks, or to avoid unnecessary ones. The scientific basis for this approach has been documented and feasibility demonstrated (*1*).

Economic analysis of cardiac PET using ^{82}Rb for symptomatic or asymptomatic subjects with coronary atherosclerosis demonstrates that it is less expensive than the cost of SPECT stress testing and associated definitive coronary arteriography in the many normal individuals with false-positive thallium stress tests (*1*).

It is significant that in over 4,000 clinical cardiac PET studies at university and private sites, over 90% of private health insurers have reimbursed fully for cardiac PET with ^{82}Rb because it is approved by the FDA and because they realize that it prevents many unnecessary coronary arteriograms and mechanical interventions while correctly identifying even asymptomatic individuals for whom such procedures are essential. Therefore, PET provides an economical basis for selective, specific medical intervention to reverse coronary atherosclerosis and/or selective mechanical intervention for severe disease to prevent myocardial infarction or sudden death.

ACKNOWLEDGMENTS

Supported in part by NIH Grants RO1-HL26862, RO1-HL42453, and RO1-HL26885 and a Joint Collaborative Research Agreement with the Clayton Foundation for Research, Houston, Texas.

REFERENCES

1. Gould KL. *Coronary artery stenosis.* New York, Elsevier Scientific Publishing, 1990.
2. Michael Fisher, ed. Guide to clinical preventive services. Report of the U.S. preventive services task force. *An assessment of the effectiveness of 169 interventions.* Baltimore: Williams and Wilkins; 1989; 3–11.
3. Olofsson BO, Bjerle P, Aberg T, Osterman G, Jacobsson KA. Prevalence of coronary artery disease in patients with valvular heart disease. *Acta Med Scand* 1985;218:365–371.
4. Langou RA, Huang EK, Kelley MJ, Cohen LS. Predictive accuracy of coronary artery calcification and abnormal exercise test for coronary artery disease in asymptomatic men. *Circulation* 1980;62(6):1196–1203.
5. Campbell S, Barry J, Rebecca GS, et al. Active transient myocardial ischemia during daily life in asymptomatic patients with positive exercise tests and coronary artery disease. *Am J Cardiol* 1986;57:1010–1016.
6. Resnekov L. Silent myocardial ischemia: Therapeutic implications. *Am J Med* 1985;79:30–34.
7. Fleg JL, Gerstenblith G, Zonderman AB, et al. Prevalence and prognostic significance of exercise induced silent myocardial ischemia detected by thallium scintigraphy and electrocardiography in asymptomatic volunteers. *Circulation* 1989;81:428–436.
8. Gottlieb SO, Weisfeldt ML, Ouyang P, Mellits ED, Gerstenblith G. Silent ischemia as a marker for early unfavorable outcomes in patients with unstable angina. *N Engl J Med* 1986;314:1214–1219.
9. Cohn PF. Clinical importance of silent myocardial ischemia in asymptomatic subjects. *Circulation* 1989;81:691–693.
10. Cohn PF. Silent myocardial ischemia: present status. *Mod Concepts CV Dis* 1987;56:1–4.
11. Younis LT, Byers S, Shaw L, Barth G, Goodgold H, Chaitman BR. Prognostic importance of silent myocardial ischemia detected by intravenous dipyridamole thallium myocardial imaging in asymptomatic patients with coronary artery disease. *J Am Coll Cardiol* 1989;14:1635–1641.
12. Brown KA, O'Meara J, Chambers CE, Plante DA. Ability of dipyridamole-thallium-201 imaging one to four days after acute myocardial infarction to predict in-hospital and late recurrent myocardial ischemic events. *Am J Cardiol* 1990;65:160–167.
13. Hendel RC, Layden JJ, Leppo JA. Prognostic value of dipyridamole thallium scintigraphy for evaluation of ischemic heart disease. *J Am Coll Cardiol* 1990;15:109–116.
14. Leppo J, Plaja J, Gionet M, Tumolo J, Paraskos JA, Cutler BS. Noninvasive evaluation of cardiac risk before elective vascular surgery. *J Am Coll Cardiol* 1987;9:269–276.
15. Midwall J, Ambrose J, Pichard A, Abedin Z, Herman MV. Angina pectoris before and after myocardial infarction. *Chest* 1982;81:681–686.
16. Reunanen A, Aromaa A, Pyorala K, Punsar S, Maatela J, Knekt P. The Social Insurance Institution's coronary heart disease study: Baseline data and 5-year mortality experience. *Acta Med Scand Suppl* 1983;673:67–81.
17. Kannel WB, Abbot RD. Incidence and prognosis of unrecognized myocardial infarction. An update on the Framingham Study. *N Engl J Med* 1984;311:1144–1147.
18. Lown B. Sudden cardiac death: The major challenge confronting contemporary cardiology. *Am J Cardiol* 1979;43:313–328.
19. Oliver MF. Strategies for preventing and screening for coronary heart disease. *Br Heart J* 1985;54:1–5.
20. Uhl GS, Froelicher V. Screening for asymptomatic coronary artery disease. *J Am Coll Cardiol* 1983;1:946–955.
21. Houck PD. Epidemiology of total cholesterol to HDL ratio in 11,669 Air Force personnel and coronary artery anatomy in 308 healthy aviators. *J Am Coll Cardiol* 1988;11:222A.
22. Love WD, Burch GE. A study in dogs of methods suitable for estimating the rate of myocardial uptake of Rb-86 in man, and the effect of norepinephrine and pitression on Rb-86 uptake. *J Clin Invest* 1957;36:468–478.
23. Yano Y, Cahoon JL, Budinger TF. A precision flow-controlled Rb-82 generator for bolus or constant-infusion studies of the heart and brain. *J Nucl Med* 1981;22:1006–1010.
24. Neirinckx RD, Kronauge JF, Gennaro GP. Evaluation of inorganic absorbents for rubidium-82 generator: I. Hydrous Sno_2. *J Nucl Med* 1982;24:898–906.
25. Mullani NA, Gould KL. First pass regional blood flow measurements with external detectors. *J Nucl Med* 1983;24:577–581.
26. Mullani NA, Goldstein RA, Gould KL, Fisher DJ, Marani SK, O'Brien HA. Myocardial perfusion with rubidium-82. I. Measurement of extraction fraction and flow with external detectors. *J Nucl Med* 1983;24:898–906.
27. Goldstein RA, Mullani NA, Fisher D, Marani S, Gould KL, O'Brien HA. Myocardial perfusion with rubidium-82. II. The effects of metabolic and pharmacologic interventions. *J Nucl Med* 1983;24:907–915.
28. Schelbert HR, Phelps ME, Huang SC, et al. N-13 ammonia as an indicator of myocardial blood flow. *Circulation* 1981;63:1259–1272.
29. Schelbert HR, Phelps ME, Hoffman EJ, Huang SC, Selin CE. Regional myocardial perfusion assessed with N-13 labeled ammonia and positron emission computerized axial tomography. *Am J Cardiol* 1979;43:209–218.
30. Yoshida K, Endo M, Himi T, et al. Measurement of regional myocardial blood flow in hypertrophic cardiomyopathy: Application of the first pass flow model using N-13 ammonia and PET. *Am J Physio Imaging* 1987;4:97–104.
31. Xu EZ, Mullani NA, Gould KL, Anderson WL. A segmented attenuation correction CSAC/for PET. *J Nucl Med*: 1990; 31:000–000.
32. Gould KL, Goldstein RA, Mullani NA, et al. Noninvasive assessment of coronary stenosis by myocardial perfusion imaging during pharmacologic coronary vasodilation. VIII. Clinical feasibility of positron cardiac imaging without a cyclotron using generator-produced rubidium-82. *J Am Coll Cardiol* 1986;7:775–789.
33. Kirkeeide RL, Gould KL, Parsel L. Assessment of coronary stenosis by myocardial perfusion imaging during pharmacologic coronary vasodilation. VII. Validation of coronary flow reserve as a single integrated functional measure of stenosis severity reflecting all its geometric dimensions. *J Am Coll Cardiol* 1986;7:103–113.
34. Gould KL. Identifying and measuring severity of coronary artery stenosis. Quantitative coronary arteriography and positron emission tomography.

Circulation 1988;68:237–245.
35. Demer LL, Gould KL, Goldstein RA, et al. Assessment of coronary artery disease severity by positron emission tomography. Comparison with quantitative arteriography in 193 patients. *Circulation* 1989;79:825–835.
36. Schelbert HR, Wisenberg G, Phelps ME, et al. Non-invasive assessment of coronary stenosis by myocardial imaging during pharmacologic coronary vasodilation. VI. Detection of coronary artery disease in man with intravenous N-13 ammonia and positron computed tomography. *Am J Cardiol* 1982;49:1197–1207.
37. Yonekura Y, Tamaki N, Senda M, et al. Detection of coronary artery disease with ammonia and high-resolution positron-emission computed tomography. *Am Heart J* 1987;113:645–654.
38. Selwyn AP, Allan RM, L'Abbate AL, et al. Relation between regional myocardial uptake of rubidium-82 and perfusion: absolute reduction of cation uptake in ischemia. *Am J Cardiol* 1982;50:112–121.
39. Deanfield JE, Shea MJ, Wilson RA, Horlock P, de Landsheere CM, Selwyn AP. Direct effects of smoking on the heart: silent ischemic disturbances of coronary flow. *Am J Cardiol* 1986;57:1005–1009.
40. Gould KL, Kirkeeide R, Buchi M. Coronary flow reserve as a physiologic measure of stenosis severity. I. Relative and absolute coronary flow reserve during changing aortic pressure. II. Determination from arteriographic stenosis dimensions under standardized conditions. *J Am Coll Cardiol* 1990;15:459–474.
41. Hicks K, Ganti G, Mullani N, Gould KL. Automated quantitation of 3D cardiac PET for routine clinical use. *J Nucl Med* 1989;30:1787–1797.
42. Gould KL. Percent coronary stenosis: Battered gold standard, pernicious relic, or clinical practicality? *J Am Coll Cardiol* 1988;11:886–888.
43. Goldstein RA, Kirkeeide R, Demer L, et al. Relations between geometric dimensions of coronary artery stenosis and myocardial perfusion reserve in man. *J Clin Invest* 1987;79:1473–1478.
44. Camici P, Araujo LI, Spinks T, et al. Increased uptake of F-18 fluorodeoxyglucose in postischemic myocardium of patients with exercise-induced angina. *Circulation* 1986;74:281–292.
45. Gould KL, Lipscomb K, Hamilton GW. A physiologic basis for assessing critical coronary stenosis: instantaneous flow response and regional distribution during coronary hyperemia as measures of coronary flow reserve. *Am J Cardiol* 1974;33:87–94.
46. Gould KL. Noninvasive assessment of coronary stenosis by myocardial imaging during coronary vasodilation. I. Physiologic principles and experimental validation. *Am J Cardiol* 1978;41:267–278.
47. Gould KL, Westcott JR, Hamilton GW. Noninvasive assessment of coronary stenosis by myocardial imaging during coronary vasodilation. II. Clinical methodology and feasibility. *Am J Cardiol* 1978;41:279–287.
48. Albro PC, Gould KL, Westcott RJ, Hamilton GW, Ritchie JL, Williams DL. Noninvasive assessment of coronary stenosis by myocardial imaging during pharmacologic coronary vasodilation. III. Clinical trial. *Am J Cardiol* 1978;42:751–760.
49. Gould KL, Kelley KO, Bolson EL. Experimental validation of quantitative coronary arteriography for determining pressure-flow characteristics of coronary stenosis. *Circulation* 1982;66:930–937.
50. Gould KL. Quantification of coronary artery stenosis in vivo. *Circ Res* 1985;57:341–353.
51. Brown BG, Bolson E, Frimer M, Dodge HT. Quantitative coronary arteriography: Estimation of dimensions, hemodynamic resistance, and atheroma mass of coronary artery lesions using the arteriogram and digital computation. *Circulation* 1977;55:329–337.
52. Marcus ML, Skorton DJ, Johnson MR, Collins SM, Harrison DG, Kerber RE. Visual estimates of percent diameter coronary stenosis: "A battered gold standard." *J Am Coll Cardiol* 1988;41:882–885.
53. White CW, Wright CB, Doty DB, et al. Does visual interpretation of the coronary arteriogram predict the physiologic importance of a coronary stenosis? *N Engl J Med* 1984;310:819–824.
54. Marcus ML, Harrison DG, White CW, McPherson DD, Wilson RF, Kerber RE. Assessing the physiologic significance of coronary obstructions in patients: Importance of diffuse undetected atherosclerosis. *Prog Cardiovasc Dis* 1988;31:39–56.
55. Sobel BE, Geltman EM, Tiefenbrunn AJ, et al. Improvement of regional myocardial metabolism after coronary thrombolysis induced with tissue-type plasminogen activator or streptokinase. *Circulation* 1984;69:983–990.
56. Tamaki N, Yonekura Y, Yamashita K, et al. Value of rest-stress myocardial positron tomography using N-13 ammonia for the preoperative prediction of reversible asynergy. *J Nucl Med* 1989;30:1302–1310.
57. Tillisch J, Brunken R, Marshall R, et al. Reversibility of cardiac wall-motion abnormalities predicted by positron tomography. *N Engl J Med* 1986;314:884–888.
58. Goldstein RA, Kirkeeide R, Smalling RW, et al. Changes in myocardial perfusion reserve after PTCA: Non-invasive assessment with positron tomography. *J Nucl Med* 1987;28:1262–1267.
59. Gould KL, Buchi M, Kirkeeide RL, Ornish D, Stein E, Brand R. Reversal of coronary artery stenosis with cholesterol lowering in man followed by arteriography and positron emission tomography [Abstract]. *J Nucl Med* 1989;30:345.
60. Ornish DM, Scherwitz LW, Brown SE, et al. Can lifestyle changes reverse atherosclerosis? *Lancet* 1990;336:129–133.
61. Schelbert HR, Buxton D. Insights into coronary artery disease gained from metabolic imaging. *Circulation* 1988;78:496–505.
62. Brunken K, Schwaiger M, Grover-McKay M, Phelps M, Tillisch J, Schelbert H. Positron emission tomography detects tissue metabolic activity in myocardial segments with persistent thallium perfusion defects. *J Am Coll Cardiol* 1987;10:557–567.
63. Goldstein RA, Mullani NA, Wong WH, et al. Positron imaging of myocardial infarction with rubidium-82. *J Nucl Med* 1986;27:1824–1829.
64. Geltman EM, Biello D, Welch MJ, et al. Characterization of transmural myocardial infarction by positron-emission tomography. *Circulation* 1982;65:747–755.
65. Schwaiger M, Brunken R, Grover-McKay M, et al. Regional myocardial metabolism in patients with acute myocardial infarction assessed by positron emission tomography. *J Am Coll Cardiol* 1986;8:800–808.
66. Marshal RC, Tillisch JH, Phelps ME, Huang SC, Carson R, Henze E, Schelbert HR. Identification and differentiation of resting myocardial ischemia and infarction in man with positron computed tomography. ^{18}F-labeled fluorodeoxyglucose and N-ammonia. *Circulation* 1983;67:766–778.
67. Brunken R, Tillisch J, Schwaiger M, Child JS, Marshall R, Mandelkern M, Phelps ME, Schelbert HR. Regional perfusion, glucose metabolism, and wall motion in patients with chronic electrocardiographic Q-wave infarctions: evidence for persistence of viable tissue in some infarct regions by positron emission tomography. *Circulation* 1986;73:951–963.
68. Ter-Pogossian MM, Klein MS, Markham J, Roberts R, Sobel BE. Regional assessment of myocardial metabolic integrity in vivo by positron-emission tomography with ^{12}C-labeled palmitate. *Circulation* 1980;61:242–255.
69. Goldstein RA. Kinetics of rubidium-82 after coronary occlusion and reperfusion. *J Clin Invest* 1985;75:1131–1137.
70. Garza D, Sease DR, Merhige ME, Hicks K, Mullani N, Gould KL. Non-invasive identification of viable versus infarcted myocardium by automated three-dimensional cardiac positron emission tomography with generator-produced rubidium-82 [Abstract]. *J Nucl Med* 1989;30:865.
71. Grover-McKay M, Schelbert HR, Schwaiger M, et al. Identification of impaired metabolic reserve by atrial pacing in patients with significant coronary artery stenosis. *Circulation* 1986;74:281–292.
72. Demer L, Gould KL, Kirkeeide R. Assessing stenosis severity: coronary flow reserve, collateral function, quantitative coronary arteriography, positron imaging, and digital subtraction angiography. A Review and Analysis. *Prog Dis* 1988;30:307–322.
73. Demer LL, Gould KL, Goldstein R, Kirkeeide RL. Non invasive assessment of coronary artery collaterals in man by PET perfusion imaging. *J Nucl Med* 1990;31:259–270.
74. Gould KL. Coronary steal—Is it clinically important? *Chest* 1989;96:227–229.
75. Kehtarnavaz N, DeFigueiredo RJP. A novel surface reconstruction and display method for cardiac PET imaging. *IEEE Trans Medical Imaging*, 1984; MI-3:108–115.
76. Gould KL. Assessment of coronary stenosis by myocardial perfusion imaging during pharmacologic coronary vasodilatation. IV. Limits of stenosis detection by idealized, experimental, cross-sectional myocardial imaging. *Am J Cardiol* 1978;42:761–768.
77. Gould KL, Lipscomb K. Effects of coronary stenosis on coronary flow reserve and resistance. *Am J Cardiol* 1974;34:48–55.
78. Gould KL, Lipscomb K, Calvert J. Compensatory changes of the distal coronary vascular bed during progressive coronary constriction. *Circulation* 1975;51:1085–1094.
79. Gould KL, Hamilton GW, Lipscomb K, Kennedy JW. A method for assessing stress-induced regional malperfusion during coronary arteriography: experimental validation and clinical application. *Am J Cardiol* 1964;34:557–564.
80. Gould KL, Schelbert HR, Phelps ME, Hoffman EJ. Noninvasive assessment of coronary stenosis with myocardial perfusion imaging during

pharmacologic coronary vasodilation. V. Detection of 47% diameter coronary stenosis with intravenous N-13 ammonia and positron emission tomography in intact dogs. *Am J Cardiol* 1979;43:200–208.
81. Gould KL. Quantification of coronary artery stenosis in vivo. *Circ Res* 1985;57:341–353.
82. Gould KL, Kelly KO, Bolson EL. Experimental validation of quantitative coronary arteriography for determining pressure-flow characteristics of coronary stenosis. *Circulation* 1982;66:930–937.
83. Gould KL, Kelly KO. Physiological significance of coronary flow velocity and changing stenosis geometry during coronary vasodilation in dogs. *Circ Res* 1982;50:695–704.
84. Gould KL. Positron tomography for heart disease: clinical update. In: Braunwald E, ed. *Heart disease, a textbook of cardiovascular medicine,* Third edition. 10th update. New York: W.B. Saunders; 1990.
85. Josephson MA, Brown BG, Hecht HS, Hopkins J, Pierce CD, Petersen R. Noninvasive detection and localization of coronary stenosis in patients: comparison of resting dipyridamole and exercise thallium-201 myocardial perfusion imaging. *Am Heart J* 1982;103:1008–1018.
86. Leppo J, Boucher CA, Okada RD, Newell JB, Strauss W, Pohost GM. Serial thallium-201 myocardial imaging after dipyridamole infusion. *Circulation* 1982;66:649–657.
87. Iskandrian AS, Heo J, Askenase A, Segal BL, Auerbach N. Dipyridamole cardiac imaging. *Am Heart J* 1988;115:432–443.
88. Leppo J. Dipyridamole-thallium imaging: the lazy man's stress test. *J Nucl Med* 1989;30:281–287.
89. Verani MS, Mahmarian JJ, Hixson JB, Boyce TM, Staudacher RA. Diagnosis of coronary artery disease by controlled coronary vasodilation with adenosine and thallium-201 scintigraphy in patients unable to exercise. *Circulation* 1990;82:80–87.
90. Brown G, Josephson MA, Peterson RB, et al. Intravenous dipyridamole combined with isometric handgrip for near maximal acute increase in coronary flow in patients with coronary artery disease. *Am J Cardiol* 1981;48:1077–1085.
91. Wilson RF, Laughlin DE, Ackell PH, et al. Transluminal subselective measurement of coronary artery blood flow velocity and vasodilator reserve in man. *Circulation* 1985;72:82–92.
92. Harrison DG, White DW, Hiratzka LF, et al. The value of lesion cross-sectional area determined by quantitative coronary angiography in assessing the physiological significance of proximal left anterior descending coronary arterial stenosis. *Circulation* 1984;69:1111–1119.
93. White CW, Wright CB, Doty DB, et al. Does visual interpretation of the coronary arteriogram predict the physiological importance of a coronary stenosis? *N Engl J Med* 1984;310;819–824.
94. Vogel RA, LeFree M, Bates E, et al. Application of digital techniques to selective coronary arteriography: use of myocardial contrast appearance time to measure coronary flow reserve. *Am Heart J* 1984;107:153–164.
95. Nissen SE, Elion JL, Booth DC, Evans J, DeMaria AN. Value and limitations of computer analysis of digital subtraction angiography in the assessment of coronary flow reserve. *Circulation* 1986;73:562–571.
96. Zijlstra F, Fioretti P, Reiber JHC, Serruys PW. Which cineangiographically assessed anatomic variable correlates best with functional measurements of stenosis severity?: a comparison of quantitative analysis of the coronary cineangiogram with measured coronary flow reserve and exercise/redistribution thallium-201 scintigraphy. *J Am Coll Cardiol* 1988; 12:686–691.
97. Blankenhorn DH, Nessim SA, Johnson RL, Sanmarco ME, Azen SP, Cashin-Hemphill L. Beneficial effects of combined colestipolniacin therapy on coronary atherosclerosis and coronary venous bypass grafts. *JAMA* 1987;257:3233–3240.
98. Brown GB, Alberts JJ, Fisher LD, et al. Niacin or Lovastatin, combined with Colestipol regresses coronary atherosclerosis and prevents clinical events in men with elevated apolipoprotein B. *N Engl J Med* 1990;323: 1289–98.
99. Turner DA. An intuitive approach to receiver operating characteristic curve analysis. *J Nucl Med* 1978;19:213–220.
100. Turner DA, Battle WE, Deshmukh H, et al. The predictive value of myocardial perfusion scintigraphy after stress in patients without previous myocardial infarction. *J Nucl Med* 1978;19:249–255.
101. Massof R, Emmel T. Criterion-free parameter-free, distribution-independent index of diagnostic test performance. *Applied Optics* 1987;26: 1395–1408.
102. Hlatky MA, Mark DB, Harrell FE, Califf RM, Pryor DB. Rethinking sensitivity and specificity. *Am J Cardiol* 1987;59:1195–1198.
103. Ritchie JL, Trobaugh GB, Hamilton GW, et al. Myocardial imaging with thallium-201 at rest and during exercise. Comparison with coronary arteriography and resting and stress electrocardiography. *Circulation* 1977;56:66–78.
104. Ritchie JL, Zaret BL, Strauss HW, et al. Myocardial imaging with thallium-201: A multicenter study in patients with angina pectoris or acute myocardial infarction. *Am J Cardiol* 1978;42:345–350.
105. Maddahi J, Garcia EV, Berman DS, Waxman A, Swan HJC, Forrester J. Improved non-invasive assessment of coronary artery disease by quantitative analysis of regional stress myocardial distribution and washout of thallium-201. *Circulation* 1981;64:924–935.
106. DePasquale EE, Nody AC, DePuey EG, et al. Quantitative rotational thallium-201 tomography for identifying and localizing coronary artery disease. *Circulation* 1988;77:316–327.
107. Van Train KF, Berman DS, Garcia EV, et al. Quantitative analysis of stress thallium-201 myocardial scintigrams: A multicenter trial. *J Nucl Med* 1986;78:17–25.
108. Ranhosky A, Gerlag DM. Quantitative interpretation provides no advantage over qualitative interpretation in intravenous dipyridamole thallium imaging. *Circulation* 1988;87:II–432.
109. Iskandrian AS, Heo J, Kong B, Lyons E. Effect of exercise level on ability of thallium-201 tomographic imaging in detecting coronary artery disease: Analysis of 461 patients. *J Am Coll Cardiol* 1989;14:1477–1486.
110. Kahn JK, McGhie I, Akers MS, et al. Quantitative rotational tomography with ^{201}Tl and ^{99m}Tc 2-methoxy-isobutyl-isonitrile. A direct comparison in normal individuals and patients with coronary artery disease. *Circulation* 1989;79:1282–293.
111. Van Train KF, Maddahi J, Berman DS, et al. Quantitative analysis of tomographic stress thallium-201 myocardial scintigrams: A multicenter trial. *J Nucl Med* 1990;31:1168–79.
112. Nolewajka AJ, Kostuk WJ, Howard J, Rechnitzer PA, Cunningham DA. thallium-201 stress myocardial imaging: an evaluation of fifty-eight asymptomatic males. *Clin Cardiol* 1981;4:134–138.
113. Schwartz RS, Jackson WG, Celio PV, Hickman JR. Exercise thallium-201 scintigraphy for detecting coronary artery disease in asymptomatic young men. *J Am Coll Cardiol* 1988;11:80A.
114. Bungo MW, Leland OS. Discordance of exercise thallium testing with coronary arteriography in patients with atypical presentations. *Chest* 1983;83:112–116.
115. Koistinen MH, Huikuri HV, Pirttiaho H, Linnaluoto MK, Takkunen JT. Evaluation of exercise electrocardiography and thallium tomographic imaging in detecting asymptomatic coronary artery disease in diabetic patients. *Br Heart J* 1990;63:7–11.
116. Gould KL. How accurate is thallium exercise testing? *J Am Coll Cardiol* 1989;14:1487–1490.
117. Gould KL. Agreement on the accuracy of thallium stress testing. *J Am Coll Cardiol* 1990;16:1022–23.
118. Diamond GA. Suspect specificity. *J Am Coll Cardiol* 1990;16:1017–21.
119. Williams BR, Jansen DE, Wong LF, Fiedotin AF, Knopf WD, Toporoff SJ. Positron emission tomography for the diagnosis of coronary artery disease: A non-university experience and correlation with coronary angiography [Abstract]. *J Nucl Med* 1989;30:845.
120. Tamaki N, Yonekura Y, Senda M, et al. Value and limitation of stress thallium-201 single photon emission computed tomography: Comparison with N-13 ammonia positron tomography. *J Nucl Med* 1988;29:1191–1188.
121. Marwick TH, Go RT, MacIntyre WJ, et al. Disparities between myocardial perfusion imaging using Rb-82 PET and T1-201 SPECT after dipyridamole stress [Abstract]. *J Nucl Med* 1989;20:861.
122. Go RT, Marwick TH, MacIntyre WJ, et al. Initial results of comparative rubidium-82 and thallium-201 myocardial perfusion imaging in diagnosis of CAD [Abstract]. *J Nucl Med* 1989;30:759.
123. Kalus ME, Stewart RE, Gacioch GM, et al. Comparison of Rb-82 PET and T1-201 SPECT for the detection of regional coronary artery disease [Abstract]. *J Nucl Med* 1989;30:829.
124. Friedman J, Van Train K, Maddahi J, et al. "Upward Creep" of the heart: a frequent source of false-positive reversible defects during thallium-201 stress-redistribution SPECT. *J Nucl Med* 1989;30:1718–1722.
125. Gould KL, Gordon DG. In: Zipes DP, Rowlands DJ, eds. *PET and clinical cardiology in progress in cardiology.* Philadelphia: Lea and Febiger; 1990.
126. Lyle FM, Gordon DG. The importance of timing with Rb-82 PET imaging of the heart [Abstract]. *J Nucl Med* 1989;30:871.
127. Senda M, Yonekura Y, Tamaki N, et al. Axial resolution and the value of interpolating scan in multislice positron computed tomography. *IEEE Trans on Medical Imaging* 1985; MI-4;44–51.
128. Mullani NA, Gould KL, Hartz RK, et al. Design and performance of

Posicam 6.5 BGO Positron Camera. *J Nucl Med* 1990;31:610–616.
129. Raylman RR, Hutchins GD, Schwaiger M, Paradise AH. The effect of axial sampling and motion on three-dimensional quantification of myocardial defects with positron emission tomography. *J Nucl Med* 1989;30: 892.
130. Bendriem B, Dewey SL, Schlyer DJ. Dependence on the recovery coefficient on axial sampling in multislice positron emission tomography. *J Nucl Med* 1989;30:892.
131. Gould KL, Goldstein RA, Mullani NA. Economic analysis of clinical positron emission tomography of the heart with rubidium-82. *J Nucl Med* 1989;30:707–717.
132. Gould KL. Goals, gold standards and accuracy of non-invasive myocardial perfusion imaging for identifying and assessing severity of coronary artery disease. *Current Opinion in Cardiology* 1989;4:834–844.
133. Gould KL, Mullani NA, Williams B. PET, PTCA and economic priorities. *Clin Cardiol* 1990;13:153–164.
134. Bodenheimer MM, Banka VS, Fooshee C, Hermann GA, Helfant RH. Relationship between regional myocardial perfusion and the presence, severity and reversibility of asynergy in patients with coronary heart disease. *Circulation* 1978;58:789–878.
135. Rozanski A, Berman DS, Gray R, et al. Use of thallium-201 redistribution scintigraphy in the preoperative differentiation of reversible and nonreversible myocardial asynergy. *Circulation* 1981;64:936–944.
136. Iskandrian AS, Hakki A-H, Kane SA, Goel IP, Mudth ED, Segal BL. Rest and redistribution thallium-201 myocardial scintigraphy to predict improvement in left ventricular function after coronary arterial bypass grafting. *Am J Cardiol* 1983;51:1312–1316.
137. Cloninger KG, DePuey EG, Garcia EV, et al. Incomplete redistribution in delayed thallium-201 single proton emission computed tomographic (SPECT) images: an overestimation of myocardial scarring. *J Am Coll Cardiol* 1988;12:955–963.
138. Galli M, Bencivelli W, Pardo NF, Tavazzi L. Underestimation of residual ischemia by thallium-201 scintigraphy after myocardial infarction. *Chest* 1988;94:876–878.
139. Tamaki N, Yonekura Y, Yamashita K, et al. Relation of left ventricular perfusion and wall motion with metabolic activity in persistent defects on ^{201}Tl tomography in healed myocardial infarction. *Am J Cardiol* 1988;62:202–208.
140. Brunken RC, Kottou S, Nienaber CA, et al. PET detection of viable tissue in myocardial segments with persistent defects at Tl-201 SPECT. *Radiology* 1989;172:65–73.
141. Tamaki N, Yonekura Y, Yamashita K, et al. Positron emission tomography using fluorine-18 deoxyglucose in evaluation of coronary artery bypass grafting. *Am J Cardiol* 1989;64:860–865.
142. Hill JL, Gettes LS. Effect of acute coronary artery occlusion on local myocardial extracellular K+ activity in swine. *Circulation* 1980;61:768–777.
143. Conrad GL, Rau EE, Shine KI. Creatine kinase release, potassium-42 content and mechanical performance in anoxic rabbit myocardium. *J Clin Invest* 1979;64:155–161.
144. Gould KL, Haynie M, Hess MJ, Yoshida K, Mullani NA, Smalling RW. Myocardial metabolism of fluorodeoxyglucose compared to cell membrane integrity for the potassium analog Rb-82 for assessing viability and infarct size in man by PET. *J Nucl Med* 1990:31:1–9.
145. Sease D, Garza D, Merhige ME, et al. Does myocardial uptake of F-18-Fluoro-deoxy-glucose by positron emission tomography reliably indicate myocardial viability in acute myocardial infarction? [Abstract]. *Circulation* 1989;80:II–378.
146. Pierard LA, DeLandsheere CM, Berthe C, Rigo P, Kulbertus HE. Identification of viable myocardium by echocardiography during dobutamine infusion in patients with myocardial infarction after thrombolytic therapy: comparison with positron emission tomography. *J Am Coll Cardiol* 1990;15:1021–31.
147. Bianco JA, Bakanauskas J, Carlson M, et al. Augmented uptake of 2-C-14-D-deoxyglucose in reversibly-injured myocardium. *Eur J Nucl Med* 1988;13:557–562.
148. Komatsumoto S, Greenberg JH, Hickey WF, Reivich M. Local cerebral glucose utilization in chronic middle cerebral artery occlusion in the cat. *J Cereb Blood Flow Metab* 1989;9:535–547.
149. Wijns W, Jacque AM, Leners N, et al. Accumulation of polymorphonuclear leukocytes in reperfused ischemic canine myocardium: relation with tissue viability assessed by fluorine-18-2-Deoxyglucose uptake. *J Nucl Med* 1988;29:1826–1832.
150. Mody F, Buxton D, Krivokapich J, Hansen H, Selin C, Schelbert H. Attenuated response of glucose metabolism in reperfused canine myocardium to changes in substrate levels. *J Am Coll Cardiol* 1990;15:80A.
151. Merhige ME, Ekas RD, Mossberg K, Taegtmeyer HT, Gould KL. Catechol stimulation, substrate competition and myocardial glucose uptake in conscious dogs assessed with positron emission tomography. *Circ Res* 1987;61(supp II):124–120.
152. Bonow RO, Bacharach SL, Cuocolo A, Dilsizian V. Myocardial viability in coronary artery disease and left ventricular dysfunction: thallium-201 reinjection vs fluorodeoxyglucose [Abstract]. *Circulation* 1989;80: (suppl) II–377.
153. Bonow RO, Dilsizian V, Cuocolo A, Bacharach SL. Myocardial viability in patients with chronic coronary artery disease and left ventricular dysfunction: thallium-201 reinjection versus ^{18}F-fluorodeoxyglucose. *Circulation* (In Press).

EDITORIAL

The Clinical Role of Positron Emission Tomography for Cardiology in the 1990s and Beyond

Although positron emission tomography (PET) has been performed in patients for more than 15 years, it has only recently begun to emerge as a diagnostic modality for use by clinicians. Implementation of clinical PET has been delayed by several factors, including the high cost of required equipment ($5–7 million with camera, cyclotron and supporting equipment), absence of U.S. Food and Drug Administration (FDA) approval, the lack of widespread reimbursement from federal and private insurers, and the paucity of large clinical trials (including outcome data) from multiple sites. Some solutions to these limitations appear to be near. The entry of major manufacturers into PET imaging should decrease the price of cameras due to increased competition. Other recent changes are joint ventures between clinical and/or research centers with radiopharmaceutical groups that share a cyclotron. By sharing or leasing the cyclotron, the capital equipment and operating costs should be reduced while making PET tracers available to sites with cameras but without cyclotrons. The regulatory barriers are also starting to resolve. In November 1989, the FDA issued a position statement on PET radiopharmaceuticals indicating that PET centers could continue to operate even though New Drug Applications

Received Jan. 17, 1991.
For reprints contact: Richard A. Goldstein, MD, Director, Nuclear Cardiology, Cardiology Division Room 1.246, The University of Texas Medical School at Houston, 6431 Fannin, Houston, TX 77030.